Draft version June 2, 2021
Typeset using LaTeX **preprint** style in AASTeX63

EPRV Sims Technical Report

Patrick D Newman,[1] Peter Plavchan,[1] Jennifer A. Burt,[2] Johanna Teske,[3]
Eric E. Mamajek,[2] Stephanie Leifer,[4] Scott Gaudi,[5] and Gary Blackwood[2]

[1] *Department of Physics and Astronomy, George Mason University, 4400 University Drive, MSN 3F3, Fairfax, VA 22030*

[2] *Jet Propulsion Laboratory, California Institute of Technology, 4800 Oak Grove Dr., Pasadena, CA 91109, USA*

[3] *Carnegie Institution for Science, Earth and Planets Laboratory, 5241 Broad Branch Road, NW, Washington, DC 20015*

[4] *The Aerospace Corporation, 200 S Los Robles Ave #150, Pasadena, CA 91101*

[5] *The Ohio State University, Columbus, OH*

(Dated: June 2, 2021)

Contents

pnewman8@masonlive.gmu.edu

1. OVERVIEW

1.1. *Document Purpose and Scope*

The National Academies Exoplanet Science Strategy (ESS) report in 2018 recommended that "NASA and NSF should establish a strategic initiative in extremely precise radial velocities (EPRVs) to develop methods and facilities for measuring the masses of temperate terrestrial planets orbiting Sun-like stars". In response, NASA and the NSF established the Extreme Precision Radial Velocity (EPRV) Working Group in 2019 to "recommend a ground-based program architecture and implementation plan accounting for the full scope of the ESS report findings" (Terms of Reference for an EPRV Working Group).

As a first step, the Working Group established a set of requirements that any future, ground-based, EPRV survey must be able to achieve in order to be considered successful. First among these was a demonstration of the ability to survey a sample of likely direct imaging targets stars in an effort to detect and characterize "Earth-like" planets. That is, the stars must be surveyed in such a way that the resulting RV data allows for the determination of a 10σ minimum mass measurement (m·sin(i)) for $1M_\oplus$ exoplanet orbiting a Sun-like star such that it receives $\pm10\%$ of the Earth's insolation level. This corresponds to approximately a 1 cm/s uncertainty for 10 cm/s velocity semi-amplitude signals. Additionally, the survey must be completed prior to the late-2030s launch of future direct imaging mission concepts such as HabEx and LUVOIR.

Members of the Working Group were tasked with designing a variety of survey architectures that might be able to meet these performance requirements. The head of each architecture, its "Champion", proposed unique combinations of telescope apertures, spectrograph parameters, and survey strategies. To evaluate the relative success of the different architectures, the EPRV Working Group established a survey strategy sub-group "E" co-chaired by Johanna Teske and Jennifer Burt. The survey strategy sub-group generated a series of EPRV survey simulations for each architecture to quantitatively evaluate their relative strengths and weaknesses. Other sub-groups evaluated additional aspects of the architectures, such as their relative costs and risks, and the outcomes from those efforts are detailed in the Working Group's final report.

Due to the limitations of the duration of the Working Group, the analysis presented herein was restricted to simulating realistic cadences of each architecture survey for a given sample of known targets. No injection and recovery tests with realistic exoplanet populations and stellar activity were performed on the resulting simulated data, but such efforts could be the subject of future work. Rather, we use the theoretical best-case scenario for estimating the detection significance achieved for a 1 $M_\oplus$ planet in an edge-on, circular, 1 *au* orbit around a 1 M Sun-like star (Gaudi & Winn 2007)

$$SNR = \frac{K}{\sigma}\sqrt{\frac{N_{\rm obs}}{2}} \tag{1}$$

where K is the stellar reflex velocity semi-amplitude due to the orbiting exoplanet, σ is the typical single measurement precision, and $N_{\rm obs}$ is the number of observations realized from our simulations over the survey duration, which is assumed to be greater than the exoplanet orbital periods of interest. In other words, throughout this analysis we assume stellar activity can be perfectly modeled and subtracted from observed RVs.

In §2, we describe the software used for the simulations, what features it considers and ignores, what inputs it needs, and what output it generates. In §3, we show the results for each architecture. In §4, we compare the figures of merit across architectures. In §5, we present a discussion of the results and limitations and effects of survey simulations, and in §**??** we present our conclusions.

2. SURVEY SIMULATION DESCRIPTION

In this section, we outline the survey simulations and the components and assumptions that went into these simulations. At the top level we simulate multiple radial velocity surveys to benchmark against one another. Each simulated radial velocity survey consists of a set of telescopes in a global network with different spectrographs and telescope specifications, which we call "architectures" (see §2.4), along with other additional miscellaneous simulation inputs (§2.6). Then for each telescope site, we simulate the observations of a set of targets (see §2.5) using a dispatch schedule that takes into account a variety of observational constraints and target prioritization (§2.1). The RV precision (§2.2) and exposure times are then simulated, and we conclude with describing the outputs from the simulations in §2.7.

2.1. *The dispatch scheduler*

All survey simulations were carried out using a dispatch scheduler that selects which target to observe next "on the fly", instead of following a preset observing schedule. The dispatch scheduler simulates a survey in moderate detail to provide a realistic observation time series. Our version[1] is derived from the MINERVA scheduler (Swift et al. 2015; Nava et al. 2015). The scheduler takes a list of targets with name, right ascension, declination, and estimated observation times as inputs, and generates a time series of observations for each target (as well as rise and set times for the Sun and each of the potential targets). It also generates a nightly summary file containing the start and end times of the night, the weather, the number of times each star was observed, the amount of time spent on each star which is impacted by the airmass at the time of observation, and whether the star was considered to be observable given our constraints. Constraints define the ordering and prioritization of targets to observe and can be divided into: weather, other natural constraints, observatory constraints, and prioritization weights. We discuss each of these in turn below. For simplicity, we do not take into account variable throughput from changing seeing conditions. However, the dispatch scheduler does account for airmass attenuation from Rayleigh-scattering.

[1] Available at https://github.com/pdn4kd/dispatch_scheduler

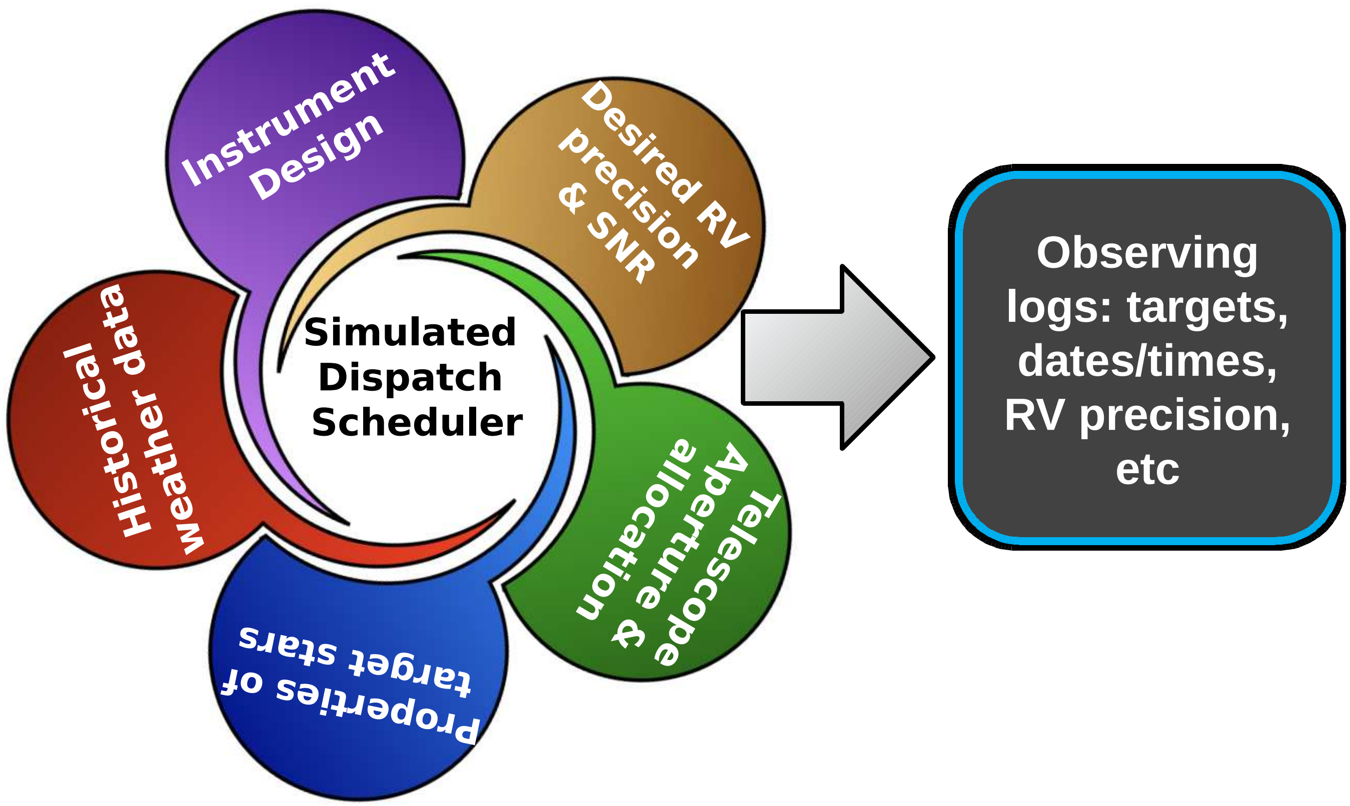

Figure 1. Outline of the simulation pipeline, including the exposure time calculator (ETC) and dispatch scheduler.

2.1.1. *Site Locations and Weather*

The architecture champions picked sites for each of the observatories in their architecture. A representative set of six locations were chosen to achieve a global network of facilities. In the final round of simulations, these locations were: Mauna Kea, Kitt Peak, and Calar Alto in the North, along with Las Campanas, Sutherland, and Siding Spring in the South. All of the architectures used all six sites. For the architectures with heterogeneous telescope compositions, the largest aperture telescopes were located at Mauna Kea and Las Campanas in our simulations.

We use historical weather records for all observatory sites in order to determine the weather during our simulated survey. For each site, we compiled either monthly, or by semester in the case of Sutherland and yearly for Siding Spring, statistics for the fraction of clear nights (Figure 2.1.1). Finally, all surveys were assumed to span 10 years in duration (2020-01-01 to 2030-01-01).

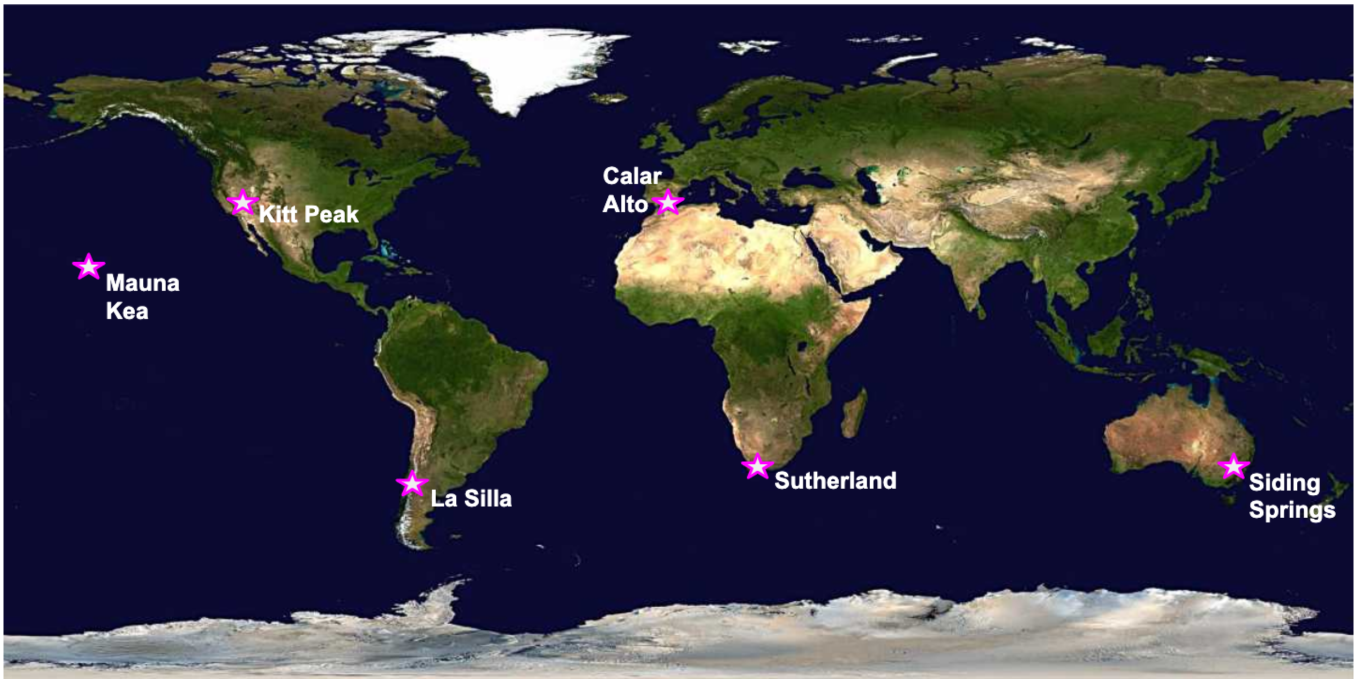

Figure 2. Site locations

We make the simplification that each night is assumed to be either entirely clear or entirely unusable, so there are no partial nights. Whether or not a night is lost due to weather is determined randomly at the start of the night, with the probabilities drawn from the historical monthly average. When monthly historical weather averages were not available, we instead used yearly averages for Siding Spring and semester averages for Sutherland. For simplification, we assume that nights lost due to weather do not exhibit night-to-night correlations, even though in reality it is typical to lose multiple nights in a row from weather patterns.

2.1.2. *Other Natural Constraints*

To further determine each target star's availability for observation we consider the telescope's latitude, longitude, and elevation, the time required for target acquisition, and the local horizon. Calculated sun-rise/set times are used to determine astronomical twilight which is when we allow observations to begin, and a minimum distance from the Moon (10 degrees) is enforced for a star to be targeted. Ephemerides for these are found via Astropy.

2.1.3. *Observatory Constraints*

For the observatory constraints, we consider telescope pointing limits (set to 30 degrees above the physical horizon), time for telescope slews between targets and for target acquisition (five minutes used for all observations), and total open shutter and detector readout times.

2.1.4. *Target Prioritization*

Finally, as per the name, we use a dispatch scheduler prioritization scheme. The scheduler determines target choices from a user provided list of stars between each observation, rather executing a preset observing order. Targets are ranked using a combination of hour angle (highest weight at zenith), and time since last observation. We assume a minimum separation between observations

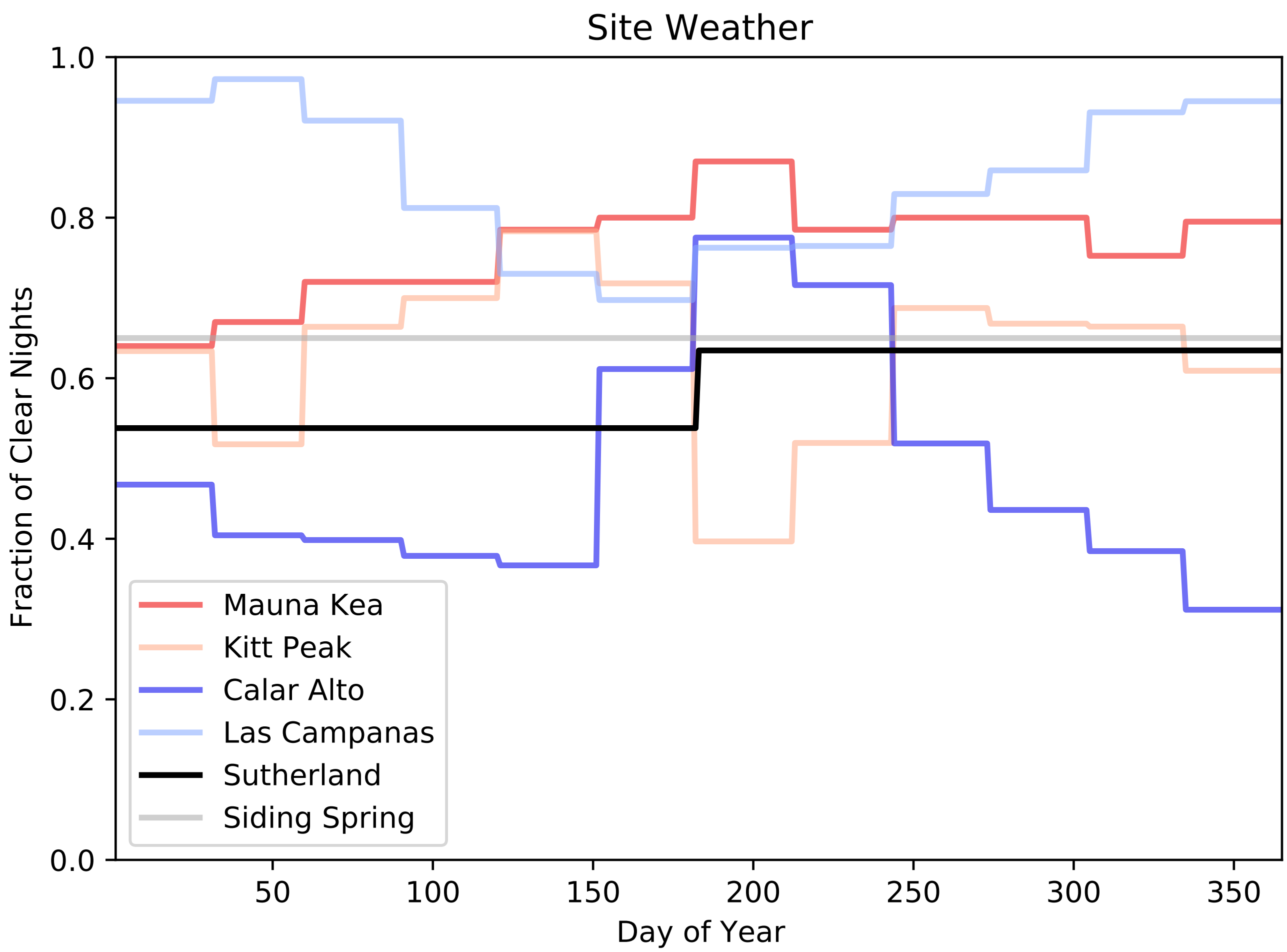

Figure 3. Nightly weather probabilities for each site included in our simulations.

of two hours (e.g. within that time the target is at a minimum priority), with linearly increasing weight thereafter. The relative weighting of these two factors can be adjusted, and we fixed the relative weighting to produce cadences that spread the observations approximately evenly between the targets (Newman in prep).

The dispatch scheduler assumes a single fixed observatory site. For handling up to the six telescope sites, a separate independent simulation was run. As such, we do not implement a mechanism for different telescope sites to coordinate prioritization of target observations with each other. In other words, we make the simplifying assumption that the telescope schedules are decoupled. On average, the different sites will randomly compensate for each others weather losses, but this is not optimized.

Despite the architectures in this survey having specified cadence goals/requirements, the dispatch scheduler does not attempt to reach any specific cadence. Rather, it observes every star in a given site's target list as frequently as possible, given the above constraints and weightings. As shown in the results, not all architectures can achieve their desired cadences. Reaching the cadences specified for each architecture below would require sculpting/optimizing the target list iteratively, which is beyond the scope and capability of these simulations.

2.2. *RV Model*

RV precision and exposure times were calculated[2] using an implementation of Beatty & Gaudi (2015). The important changes are: allowing the spectrographs defined in Section 2.4 to be in any wavelength range instead of just three specific ranges, and a simple atmospheric scattering model (Rayleigh plus a baseline). No telluric absorption is included, so our resulting RV precision estimates should be considered optimistic, especially in the near-infrared. The RV model uses a set of BT Settl synthetic stellar spectra over the user specified instrument wavelength range, and a set of pre-calculated RV precision values for each wavelength and temperature bin in units of 1 photon per m/s in each 100 Å wavelength bin as in Beatty & Gaudi (2015). Correction factors are used to account for variations in stellar log(g), metallicity, and v·sin(i).

2.3. *Exposure Time Calculations*

Exposure times at each observing site are calculated with an exposure time calculator (ETC) in two steps. First, the RV and SNR are found for an observation that is just long enough to saturate the CCD at the star's peak brightness (approximated using Wein's Law) within the spectral grasp of the spectrograph as defined in Section 2.4. Second, this exposure time is scaled to the desired RV and SNR precision based upon an assumption that we are purely photon-noise limited (RV uncertainty $\sim$ $\mathrm{SNR}^{-1} \sim \mathrm{t}^{-1/2}$). This scaling dictates how many individual exposures (co-adds) are needed, and is combined with the instrumental readout time of co-add of 30 seconds to give a cumulative ("clock") observation time.

In order to average over short term stellar pulsation modes or p-mode oscillations, we implement a minimum clock observation time of 5 minutes and execute additional exposures as needed to achieve this minimum. For simplicity, we do not adjust this minimal time to account for the estimated p-mode oscillation time as a function of individual spectral type and surface gravity for each individual target (eg: Chaplin et al. (2019)). Finally, we assume that the observatory does not move onto the next target until the final co-add is read out; conversely, this can be thought of as an additional 30-second penalty on the assumed 5 minutes for target slews and acquisition overhead.

2.4. *Architectures: Telescopes and Spectrographs*

The working group defined a set of architectures spanning a realistic set of feasible combinations of dedicated telescopes with a range of diameters and high-resolution spectrometers to meet the objectives of a next-generation global EPRV survey to search for and detect Earth-mass twins. The majority of observing architectures utilized the same notional "baseline instrument" design: a high resolution, optical band pass, extreme precision RV spectrograph loosely based on the design of NN-Explore's NEID spectrograph located on the 3.5 m WIYN telescope (Robertson et al. 2016; Schwab et al. 2016), with the remaining architectures specifying "defined instrument" variations to these spectrograph parameters. Each architecture site was generally also equipped with a 10 cm solar telescope to carry out high cadence, high SNR, day-time observations of the Sun, which is not accounted for in our simulations. In the following sub-sections, we describe each architecture in detail.

[2] Available at https://github.com/pdn4kd/reimagined-palm-tree.

Architecture	I	IIa	IIb	V
Champion	Jennifer Burt	Andrew Howard	Andrew Howard	Chas Beichman
Telescopes	6x2.4 m	2x6 m and 4x4 m	6x4 m	6x3 m
Collecting area by aperture	2.4 m = 4.2 m^2	4 m = 9.5 m^2; 6 m = 27 m^2	4 m = 9.5 m^2	3 m = 6.3 m^2
Time allocation	100%	100%	100%	100%
Wavelength coverage	380-930 nm	380 - 930 nm	380 - 930 nm	500-1700 nm
Spectral resolution	180 000	180 000	180 000	180 000
Total system efficiency	6%	6%	6%	7%
instrument noise floor	10 cm/s	5 cm/s	5 cm/s	10 cm/s
Required (peak) SNR/pix	300	300	300	300
Required RV precision	10 cm/s	10 cm/s	10 cm/s	10 cm/s
Observation cadence per star	1 / night	3 / night	3 / night	2 / telescope / night

Architecture	VI	VIIIa	VIIIb
Champion	Peter Plavchan	Benjamin Fulton	Benjamin Fulton
Telescopes	6x arrays of 1 m	2x10 m and 4x 3.5 m	2x10 m and 6x2.4 m
Collecting area by aperture	0.61m^2 each; array is 9.5 m^2	10 m = 75 m^2; 3.5 m = 9.5 m^2	10 m = 75 m^2; 2.4 m = 4.2 m^2
Time allocation	100%	25% of 10 m; 100% of 3.5m	25% of 10 m; 100% of 2.4 m
Wavelength coverage	500-800 nm	380-930 nm	380-930 nm
Spectral resolution	150 000	180 000	180 000
Total system efficiency	6%	6%	6%
instrument noise floor	10 cm/s	5 cm/s	5cm/s
Required (peak) SNR/pix	300	1000 for the 10 m; 300 for 3.5 m	1000 for the 10 m; 300 for 2.4 m
Required RV precision	10 cm/s	15 cm/s on 3.5 m; 5 cm/s on 10 m	15 cm/s on 2.4 m; 5 cm/s on 10 m
Observation cadence per star	1/night	1/week on 10 m; 1/night on 3.5 m	1/week on 10 m; 1/night on 2.4 m

Table 1. Champion defined architectures and their facility and instrumental properties. Architectures not listed (III, IV) were dropped from direct consideration in earlier simulations. Architectures with a/b variants have different sizes/numbers of telescopes, but identical instruments for each variant.

2.4.1. *Architecture I*

This architecture utilizes a network of six identical, robotic, 2.4m telescopes based on the design of the Automated Planet Finder telescope (Vogt et al. 2014) each of which is paired with one of the standardized EPRV spectrographs described above. The APF is a fully automated, robotic facility that has been executing precise RV surveys since 2014 and is the largest aperture robotic RV telescope currently in operation. The telescopes in this architecture are thus similarly dedicated robotic facilities, spending 100% of nightly observations on the EPRV survey (the survey targets are described in 2.5), along with a select set of radial velocity standard stars. As with most architectures, the telescopes are spread across both longitude and latitude - three in the northern hemisphere (Mauna Kea in Hawaii, Kitt Peak in Arizona, and Calar Alto in Spain) and three in the southern hemisphere (La Silla in Chile, Southerland in South Africa, and Siding Springs in Australia). This architecture could potentially save costs from the identical telescope hardware.

2.4.2. *Architecture II*

Architecture II employs facilities at the same locations as Architecture I but uses larger aperture telescopes. It consists of two sub-architecture variations: IIa places 6-m telescopes at Mauna Kea and Las Campanas, and 4-m telescopes at the remaining locations, while IIb uses 4-m telescopes at all six sites. Like the telescopes in architecture I, all facilities in Architecture II are dedicated and spend the entirety of their observing time working on this particular survey. Given the number of existing 4-m class telescopes, this architecture may more easily re-purpose existing observatories.

2.4.3. *Architectures III and IV*

Architecture III consists of two 10-m class telescopes, one in the Northern hemisphere and one in the South, each of which has 50% of its time assigned to carrying out this EPRV survey, matching the 10-m portion of Architecture VIII. Architecture IV is a copy of Architecture VIII, with a small fraction of additional time on one or two 25-m class telescopes that is used exclusively for RV follow-up of transiting exoplanets, and not for the primary RV survey being simulated herein. Thus, the simulated RV survey performances of Architectures III and IV can be evaluated from the simulated performance of Architecture VIII.

2.4.4. *Architecture V*

The distinguishing feature of architecture V is the spectrograph, which uses single mode fibers and extends farther into the near-infrared than its counterparts. Many of the unique advantages and challenges of this architecture are simulated at low fidelity or are outside of the scope of these simulations. For the simulations, we assume six 3-m telescopes are used.

2.4.5. *Architecture VI*

This architecture uses a fiber multi-plexed array of small (nominally 1-m) telescopes at each telescope site to get the light gathering power equivalent of a larger aperture at potentially lower cost. As simulated, each array is considered to be the same as a single 4-m class telescope (equivalent to architecture IIb). The spectrograph suffers from reduced spectral grasp and lower spectral resolution due to the penalty of multiple fibers for each telescope in the array, and drives the difference in the assumed instrument parameters.

2.4.6. *Architecture VIII*

Architecture VIII is explicitly a hybrid architecture. It combines a pair of 10-m class telescopes operating at high precision and limited time allocation, one in each hemisphere, and a larger number (4-6) of smaller telescopes at lower precision and 100% dedicated time allocation to the EPRV survey. Architecture VIII is the only architecture simulated with varying precision and/or varying amounts of allocated survey time available at each telescope site. The VIIIa variant has four 3.5-m telescopes (comparable to architectures IIa/b and VI) located at four other locations distinct from the two 10-m telescopes. The VIIIb variant has six 2.4 m telescopes (similar to architecture I). We simulate two telescopes each (one 10-m and one 2.4-m) at both Mauna Kea and Las Campanas. In reality, these pairs of telescopes at Mauna Kea and Las Campanas would suffer identical weather losses. However, since we simulate each telescope independently, the telescopes at the same site have independently drawn weather losses. We reuse the 10-m simulations for all of Architectures VIIIa, VIIIb, and III.

2.5. *Target Star Lists*

Future exoplanet direct imaging NASA mission concept studies have produced prioritized target lists of nearby, bright stars. To identify a set of stars that would constitute a reasonable set of targets for a future EPRV survey of direct imaging targets, we cross-matched the HabEx and LUVOIR-A, LUVOIR-B, and Starshade Rendezvous target lists (Gaudi et al. 2020; The LUVOIR Team 2019), and gathered archival information on stellar properties relevant to each star's RV information content (e.g., spectral type, effective temperature, apparent magnitude, rotational velocity, metallicity and surface gravity). After several face-to-face meetings, virtual meetings, and email correspondence, the EPRV working group reached consensus on the three target prioritization levels listed below. All stars on the green and yellow lists must satisfy the criteria that 1) planets in the habitable zone would be visible to future direct imaging efforts, and 2) the host stars themselves are amenable to EPRV observations:

- Green targets
  - Spectral types F7-K9
  - vsini $<$ 5 km/s
  - HabEx deep or nearest 50 or on N $\geq$ 2 lists (including LUVOIR-A, LUVOIR-B, HabEx, Starshade Rendezvous)
- Yellow targets
  - Spectral types F7-M
  - vsini $<$ 10 km/s
  - Appears on at least 1 study list, but not a "green" target
- Red targets
  - Spectral type hotter than F7 and/or
  - vsini $>$ 10 km/s

The green targets were designated by the EPRV working group as "musts" for an EPRV survey, while the yellow targets were designated as "wants". The red targets were excluded from consideration for the future EPRV survey simulation due to inadequate RV information content. An additional five stars were removed from the green target list to generate a "green prime" list of 101 stars. These five stars possessed the longest (in the green list) estimated exposure times from §1.4 to reach the desired RV precision, primarily due to a combination of spectral type and rotational velocity (e.g. these were corner cases). The resulting "green prime" star list (101 stars) and associated stellar properties are listed in Table 2, shown distributed on the sky in Figure 4, and constitute the sample used for our RV survey simulations.

The green prime list of targets was in turn broken into a northern hemisphere sub-set ($\geq$ -5° dec, 51 stars), and a southern hemisphere sub-set ($\leq$ +5° dec, 58 stars) for observing with telescopes in their respective hemispheres, with 9 stars near the celestial equator appearing on both lists for cross-comparison. Since our simulations do not coordinate telescope target optimization, we did not dynamically optimize which stars were observed by which telescopes (e.g. a fluid declination cutoff that is optimized for each observing site and time of year). These particular declination cuts were chosen by consensus by the EPRV Working Group to have non-zero overlap between the target lists of both hemispheres.

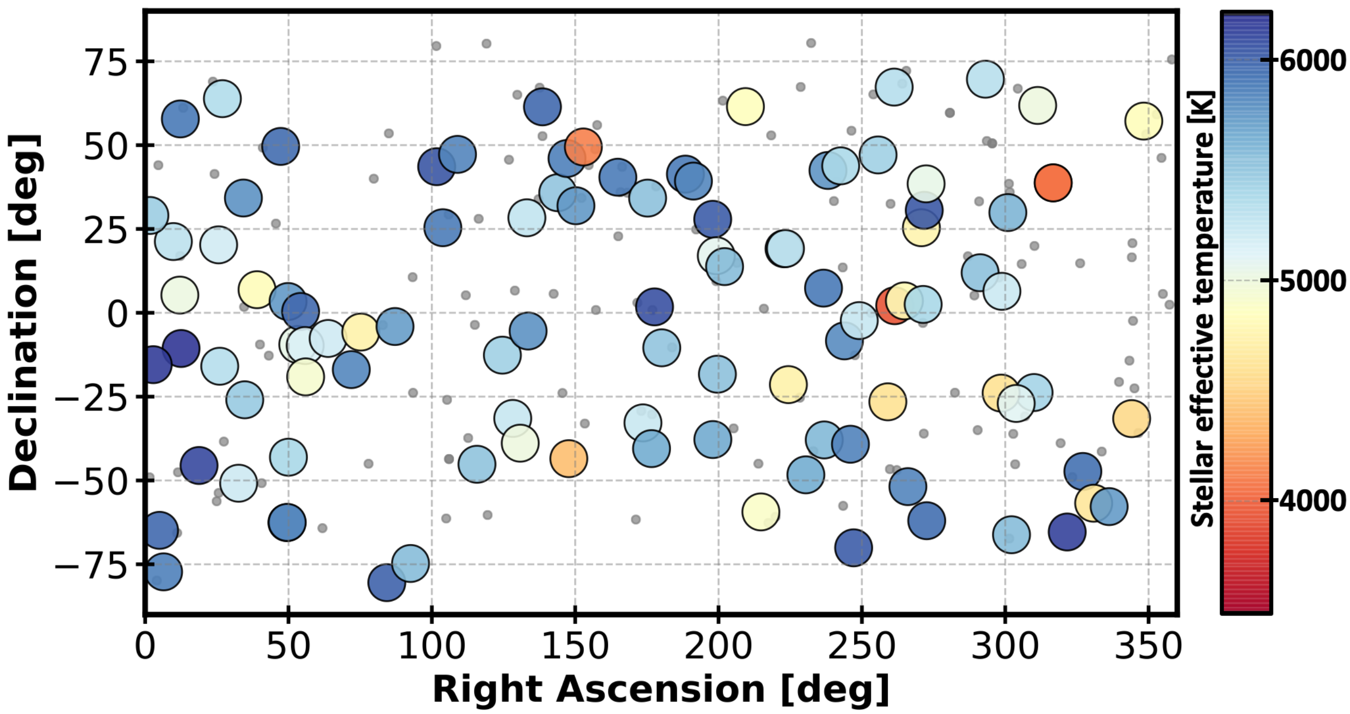

Figure 4. The locations on the sky of all green and yellow list stars. Open circles represent green list targets, color coded by effective temperature, while the yellow list stars are depicted by the grey points. While the thin disk of nearby stars is effectively isotropic on the sky, the green prime list of 101 nearby bright stars shows some minor clustering on the sky which can impact RV survey efficiency.

Table 2. Stars in the “green prime” list. Name, spectral type, and properties used in the simulations are included.

Name	Right Ascension	Declination	Distance (pc)	$v\sin i$	Spectral Type	T_{eff}	log(g)	Metallicity	Radius (R)	Hemisphere
HIP 10138	02:10:24.00	-50:49:31.1	10.787	1.9	K1.5V	5217	4.56	-0.23	0.755	South
HIP 101997	20:40:11.44	-23:46:30.0	14.677	1.8	G7.5IV-V	5414	4.46	-0.31	0.951	South
HIP 102422	20:45:17.27	+61:50:12.5	14.265	1.7	K0IV	5002	3.43	-0.09	10.188	North
HIP 104214	21:06:50.84	+38:44:29.4	3.497	1.8	K5V	4339	4.43	-0.33	1.019	North
HIP 104217	21:06:52.19	+38:44:03.9	3.495	1.8	K7V	4045	4.53	-0.38	0.809	North
HIP 105858	21:26:26.49	-65:22:05.3	9.262	3.4	F9V Fe-1.4 CH-0.7	6150	4.35	-0.66	1.225	South
HIP 10644	02:17:02.42	+34:13:29.4	11.008	2	G0.5V Fe-0.5	5786	4.29	-0.53	1.406	North
HIP 107649	21:48:15.61	-47:18:10.4	15.561	1.8	G0V Fe+0.4	5946	4.48	0.01	0.908	South
HIP 10798	02:18:58.65	-25:56:48.4	12.834	2.7	G8V	5476	4.61	-0.45	0.673	South
HIP 108870	22:03:17.44	-56:46:47.3	3.639	1.4	K4V(k)	4649	4.63	-0.19	0.643	South
HIP 110649	22:24:56.19	-57:47:47.8	20.454	1.8	G2IV-V	5739	4.15	0.05	1.941	South
HIP 113283	22:56:23.83	-31:33:54.6	7.608	2.6	K4Ve	4555	4.53	-0.01	0.809	South
HIP 114622	23:13:14.74	+57:10:03.5	6.532	1.8	K3V	4833	4.59	0	0.705	North
HIP 12114	02:36:03.83	+06:53:00.1	7.235	1.3	K3V	4829	4.6	-0.16	0.689	North
HIP 14632	03:09:02.88	+49:36:48.6	10.541	3.6	G0V	5968	4.19	0.08	1.770	North
HIP 15330	03:17:44.47	-62:34:36.8	12.039	2.7	G2.5V Hdel1	5712	4.48	-0.24	0.908	South
HIP 15371	03:18:11.14	-62:30:28.6	12.046	2.7	G1V	5852	4.43	-0.25	1.019	South
HIP 15457	03:19:21.54	+03:22:11.9	9.14	4.5	G5V	5749	4.51	0.08	0.847	Both
HIP 15510	03:19:53.22	-43:04:17.6	6.043	0.9	G6V	5398	4.41	-0.41	1.067	South
HIP 1599	00:20:01.91	-64:52:39.4	8.587	4.9	F9.5V	5977	4.51	-0.18	0.847	South
HIP 16537	03:32:56.42	-09:27:29.9	3.216	1.9	K2V	5050	4.6	-0.09	0.689	South
HIP 16852	03:36:52.52	+00:24:10.2	13.963	3.7	F9IV-V	5971	4.06	-0.09	2.388	Both
HIP 17378	03:43:14.96	-09:45:54.7	9.041	1	K0+IV	5144	3.95	0	3.077	South
HIP 17420	03:43:55.15	-19:06:40.6	13.955	3	K2.5V	4930	4.41	-0.17	1.067	South

Table 2 *continued on next page*

Table 2 *(continued)*

HIP 19849	04:15:17.64	-07:38:40.4	4.985	0.9	K0.5V	5202	4.55	-0.28	0.773	South
HIP 2021	00:25:39.20	-77:15:18.1	7.459	3.4	G0V	5873	3.98	-0.04	2.871	South
HIP 22263	04:47:36.21	-16:56:05.5	13.241	2.9	G1.5V CH-0.5	5840	4.5	0.03	0.867	South
HIP 23311	05:00:48.68	-05:45:03.5	8.848	1.4	K3+V	4745	4.57	0.19	0.738	South
HIP 26394	05:37:08.79	-80:28:18.0	18.28	2.7	G0V	6003	4.42	0.09	1.042	South
HIP 27435	05:48:34.90	-04:05:38.7	15.255	2.7	G2V	5733	4.51	-0.22	0.847	Both
HIP 29271	06:10:14.20	-74:45:09.1	10.215	2.3	G7V	5569	4.43	0.11	1.019	South
HIP 3093	00:39:22.09	+21:15:04.9	11.137	1.8	K0.5V	5303	4.56	0.18	0.755	North
HIP 32480	06:46:44.34	+43:34:37.3	16.648	3.6	F9V	6064	4.33	0.12	1.283	North
HIP 32984	06:52:18.37	-05:10:25.3	8.749	2.7	K3.5V	4758	4.5	-0.07	0.867	South
HIP 33277	06:55:18.69	+25:22:32.3	17.47	2.9	G0V	5891	4.36	-0.18	1.197	North
HIP 35136	07:15:50.11	+47:14:25.5	16.867	2.9	F9V	5849	4.26	-0.33	1.507	North
HIP 37606	07:42:57.16	-45:10:18.4	22.473	4.3	G8IV-V	5526	4.1	0.19	2.178	South
HIP 3765	00:48:22.53	+05:17:00.2	7.435	1.8	K2V	5015	4.6	-0.31	0.689	North
HIP 3821	00:49:05.10	+57:48:59.6	5.953	3.4	F9V	5904	4.32	-0.25	1.312	North
HIP 3909	00:50:07.72	-10:38:37.6	15.88	3.9	F7V	6203	4.27	-0.15	1.473	South
HIP 40693	08:18:23.78	-12:37:47.2	12.564	2.2	G8+V	5442	4.53	-0.02	0.809	South
HIP 41926	08:32:52.26	-31:30:09.7	12.182	1.8	K1V	5243	4.46	-0.41	0.951	South
HIP 42808	08:43:18.26	-38:52:59.5	11.186	2.7	K2.5V(k)	5005	4.61	-0.01	0.673	South
HIP 43587	08:52:36.13	+28:19:53.0	12.59	2.2	K0IV-V	5270	4.31	0.31	1.343	North
HIP 43726	08:54:18.19	-05:26:04.3	16.85	2.4	G2V	5781	4.44	0.12	0.996	South
HIP 45333	09:14:20.55	+61:25:24.2	19.659	4.8	G0IV-V	5973	4.13	0.05	2.033	North
HIP 47080	09:35:40.03	+35:48:38.8	11.203	2.3	G8Va	5511	4.46	0.28	0.951	North
HIP 48113	09:48:35.18	+46:01:16.4	18.904	2.9	G0.5Va	5872	4.1	0.09	2.178	North
HIP 48331	09:51:06.68	-43:30:05.9	11.285	0.9	K6V(k)	4400	4.36	-0.26	1.197	South
HIP 49081	10:01:01.02	+31:55:29.0	14.926	1.8	G3Va Hdel1	5753	4.3	0.26	1.374	North
HIP 49908	10:11:23.36	+49:27:19.7	4.869	2.7	K7V	4131	4.61	0.24	0.673	North
HIP 53721	10:59:28.22	+40:25:48.4	13.802	3.1	G1-V Fe-0.5	5894	4.3	0.02	1.374	North
HIP 544	00:06:36.53	+29:01:19.0	13.779	3.6	G8V	5458	4.52	0.14	0.828	North
HIP 56452	11:34:29.95	-32:50:00.0	9.544	0.9	K0-V	5241	4.59	-0.37	0.705	South
HIP 56997	11:41:03.03	+34:12:09.2	9.579	2.3	G8V	5528	4.53	-0.05	0.809	North
HIP 57443	11:46:32.25	-40:30:04.8	9.292	2.7	G2V	5655	4.44	-0.29	0.996	South
HIP 57757	11:50:41.29	+01:45:55.4	10.929	3.6	F9V	6083	4.08	0.24	2.281	Both
HIP 58576	12:00:44.37	-10:26:41.4	12.697	1.8	G8IV	5510	4.33	0.25	1.283	South
HIP 5862	01:15:10.57	-45:31:55.5	15.177	4.7	F9V Fe+0.4	6111	4.36	0.17	1.197	South
HIP 61317	12:33:45.09	+41:21:24.4	8.44	2.8	G0V	5887	4.34	-0.2	1.253	North
HIP 62207	12:44:59.68	+39:16:42.9	17.565	1.8	F9V Fe-0.3	5842	4.33	-0.5	1.283	North
HIP 64394	13:11:52.92	+27:52:33.7	9.129	4.5	F9.5V	6034	4.44	0.06	0.996	North
HIP 64408	13:12:03.47	-37:48:11.3	20.295	2.7	G4IV	5670	3.9	0.16	3.452	South
HIP 64797	13:16:50.67	+17:01:04.1	10.985	3.3	K2.5V(k)	5081	4.62	-0.16	0.658	North
HIP 64924	13:18:24.97	-18:18:31.0	8.555	1.8	G6.5V	5537	4.38	-0.03	1.143	South
HIP 65721	13:28:25.95	+13:46:48.7	17.91	3	G4V-IV	5559	4.05	-0.06	2.444	North
HIP 68184	13:57:32.10	+61:29:32.4	10.078	2	K3V	4851	4.58	0.11	0.721	North
HIP 69972	14:19:05.36	-59:22:37.4	11.841	0.9	K3IV	4903	4.69	0.32	0.560	South
HIP 72659	14:51:23.28	+19:06:02.3	6.733	3.5	G7V	5527	4.6	-0.13	0.689	North
HIP 72848	14:53:24.04	+19:09:08.2	11.51	3.9	K0.5V	5291	4.55	0.08	0.773	North
HIP 73184	14:57:27.35	-21:24:40.6	5.882	3.5	K4V	4744	4.76	0.12	0.477	South
HIP 75181	15:21:49.57	-48:19:01.1	14.688	2.4	G2-V	5664	4.39	-0.34	1.117	South
HIP 77257	15:46:26.75	+07:21:11.7	11.819	3.3	G0-V	5900	4.17	-0.01	1.854	North
HIP 77358	15:47:29.41	-37:54:56.9	15.26	1.8	G7IV-V	5584	4.4	0.08	1.092	South
HIP 77760	15:52:40.19	+42:27:00.0	15.832	3.4	G0V Fe-0.8 CH-0.5	5776	3.83	-0.51	4.056	North
HIP 79248	16:10:24.21	+43:49:06.1	17.942	2.6	K0V	5388	4.52	0.46	0.828	North
HIP 79672	16:15:37.13	-08:22:05.7	14.131	2.7	G2Va	5814	4.45	0.06	0.973	South
HIP 7981	01:42:29.95	+20:16:12.5	7.605	0.1	K1V	5196	4.5	-0.01	0.867	North
HIP 80337	16:24:01.24	-39:11:34.8	12.908	2.2	G1V CH-0.4	5858	4.5	0.03	0.867	South
HIP 80686	16:28:27.80	-70:05:04.8	12.177	2.4	F9V	6030	4.43	-0.08	1.019	South
HIP 8102	01:44:05.13	-15:56:22.4	3.65	0.9	G8V	5331	4.44	-0.49	0.996	South
HIP 81300	16:36:21.18	-02:19:25.8	9.92	1.6	K0V(k)	5248	4.55	0.01	0.773	Both
HIP 83389	17:02:36.30	+47:04:47.3	18.294	1.8	G8V	5442	4.39	-0.13	1.117	North
HIP 8362	01:47:44.06	+63:51:11.2	10.043	0.9	G9V	5354	4.53	0.03	0.809	North
HIP 84478	17:16:13.68	-26:32:36.3	5.95	3.3	K5V(k)	4600	4.7	-0.34	0.547	South
HIP 85235	17:25:00.90	+67:18:24.1	12.793	1.3	K0V	5327	4.56	-0.42	0.755	North

Table 2 *continued on next page*

Table 2 *(continued)*

HIP 85295	17:25:45.57	+02:06:51.5	7.715	3.5	K7V	3941	4.68	0.19	0.573	Both
HIP 86400	17:39:17.02	+03:33:19.7	11	1.5	K3-V	4808	4.56	-0.08	0.755	Both
HIP 86796	17:44:08.72	-51:50:00.9	15.605	3.8	G3IV-V	5845	4.27	0.35	1.473	South
HIP 88601	18:05:27.21	+02:30:08.8	5.123	3.7	K0-V	5394	4.56	0.07	0.755	Both
HIP 88745	18:07:01.61	+30:33:42.7	15.739	2.8	F9V mw	6049	4.18	-0.58	1.812	North
HIP 88972	18:09:37.65	+38:27:32.1	11.096	0.6	K2V	5048	4.55	-0.2	0.773	North
HIP 89042	18:10:26.26	-62:00:10.0	17.753	4.2	G0V	5950	4.31	0.01	1.343	South
HIP 910	00:11:15.91	-15:28:02.4	17.99	4.8	F8V Fe-0.8 CH-0.5	6169	4.07	-0.34	2.334	South
HIP 95447	19:24:57.77	+11:56:34.3	14.959	1.9	G7IV Hdel1	5530	4.05	0.34	2.444	North
HIP 96100	19:32:20.59	+69:39:55.4	5.755	1.8	K0V	5318	4.59	-0.15	0.705	North
HIP 97944	19:54:17.82	-23:56:24.3	14.107	1.8	K2IV(k)	4600	4.56	0.25	0.755	South
HIP 98036	19:55:18.77	+06:24:28.6	13.699	2.7	G8IV	5223	3.86	-0.17	3.785	North
HIP 98767	20:03:36.95	+29:53:53.1	16.014	0.8	G7IV-V	5606	4.44	0.25	0.996	North
HIP 99240	20:08:41.86	-66:10:45.6	6.108	2	G8IV	5566	4.24	0.32	1.578	South
HIP 99825	20:15:16.58	-27:01:57.1	8.799	0.6	K2+V	5104	4.54	0.06	0.791	South

2.6. *Other Simulation Inputs*

The architecture champions specified telescope size, available survey time (in fractions of a year), and the following instrument parameters: wavelength range, spectrograph resolution, overall efficiency, target RV precision photon noise, and target spectroscopic SNR per resolution element as specified in Table 1. The remaining parameters, all related to the detectors such as read noise and dark current (see Table 3), were kept the same across architectures. From these parameters, we calculated estimated exposure times for all stars for each telescope/site/instrument combination at an airmass of 1.0154 (10 degrees off zenith) as an intermediate step. These estimated exposure times were then scaled by the dispatch scheduler to calculate realized exposure times to achieve the desired precision. We calculated two sets of exposure times – one that accounted for only the desired photon noise RV precision, and one that met both the desired photon noise RV precision and the spectroscopic SNR per resolution element (whichever was longer), to determine which requirement was driving the simulated exposure times and consequently the achieved survey cadence.

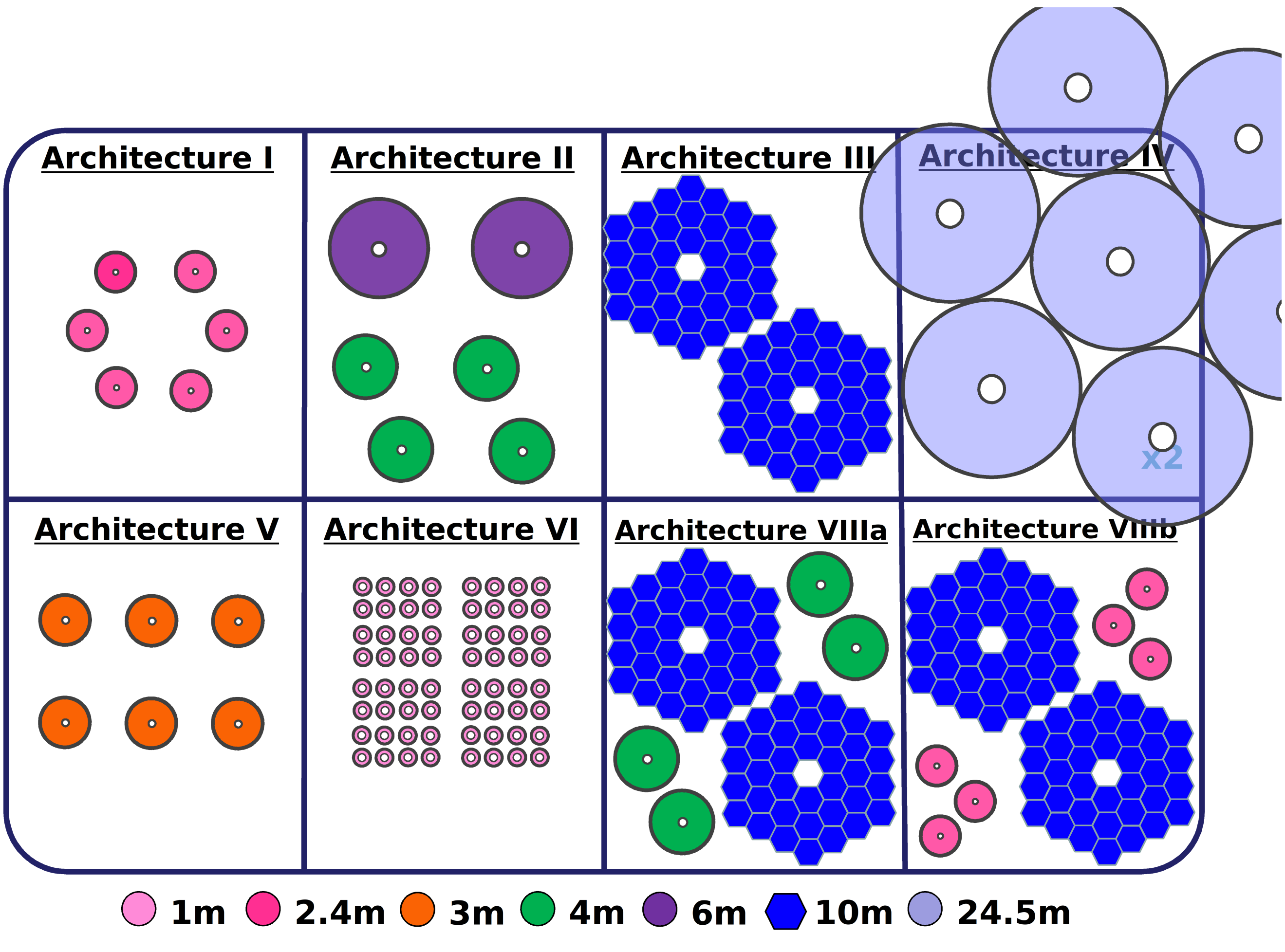

Figure 5. Representative illustration of number and diameter of telescope in the architectures.

Well Depth	Gain	Read Noise	Dark Current	Pixels per resolution element	Readout Time
90000 e-	0.704225 ADU/e-	4.5 e-	3 e-/hour	5	30 s

Table 3. Notional detector properties derived from NEID's CCDs as a representative example. These values were used for all architecture simulation spectrograph assumptions, both the defined and baseline instruments.

2.7. *Simulation Outputs*

We generate outputs from both the exposure time calculator (ETC) and the dispatch scheduler. The ETC outputs a `CSV` file, and a SIMBAD formatted `TXT` file for each run. The SIMBAD formatted `TXT` file is used as input to the dispatch scheduler (Figure 1). For all stars in a survey simulation for a given telescope in a given architecture, the ETC generated `CSV` lists one record per star containing: star name, exposure time (total elapsed clock time including readouts), sky time (open shutter time), single exposure time, number of exposures, SNR for the total exposure at a fixed airmass, and RV single measurement precision in km/s for the total exposure at a fixed airmass. The ETC-generated `TXT` contain: name, RA and Dec, exposure time (total elapsed clock time including readouts), sky time (open shutter time), single exposure time, number of exposures, and apparent V-band magnitude and spectral type. They also contain a meta-data line at the beginning of the file, with the date the file was generated, the target precision (in km/s), and the target SNR (0 for the runs where none was specified). The naming conventions are in the form "`times_architecture_site_instrument.csv`" and "`times_architecture_site_instrument.txt`". So the `CSV` of exposure times for architecture I for the telescope on Mauna Kea for a survey simulation that takes into account the minimum required SNR per spectral resolution limit in addition to (as opposed to solely) the minimum RV photon noise is named "`times_I_MK_snr.csv`".

The observation simulations from the dispatch scheduler generate the following files for each survey simulation for a given telescope in a given architecture:

- A single column of rise times for each star in individual files with file naming convention "`starnamerise.txt`"
- A single column of set times for each star in individual files with file naming convention "`starnameset.txt`"
- A single column of Sun rise times in a single file with file naming convention "`sunrise.txt`"
- A single column of Sun set times in a single file with file naming convention "`sunset.txt`"
- Observation times for each star in `CSV` formatted-files with the naming convention "`starname.txt`" containing: Observation start time (JD), observation end time (JD), open shutter observation duration (minutes), telescope altitude, telescope azimuth, observation quality (always 1 in these simulations), and number of exposures.
- Idle times in a single file named `idle.txt`. Each entry is effectively a five minute observation (defined to be at quality 0) with a single exposure, and follows the conventions of the observation times file. This file is useful for tracking the observational efficiency of a given survey, if and when no suitable survey targets are available for observing with the dispatch scheduler.
- A summary of nightly observations per target, weather, and per target observability as a single `CSV` file;
- A metadata summary file for all the instrument/site/telescope parameters used in the simulation with the naming convention "`YYYY-MM-DD.xxxxx.txt`", where "xxxxx" is the simulation run number.
- A copy of the input files used for the simulation run.

Radial velocity time-series can be generated from the observation times of each star, although that was not done here for all architectures and telescope combinations. In Figures 6, 7, and 8, we show a representative cadence and RV time-series. The full data outputs are at https://drive.google.com/open?id=12-69f-lhoY-diSzK7npP7edKZp5P1vVh

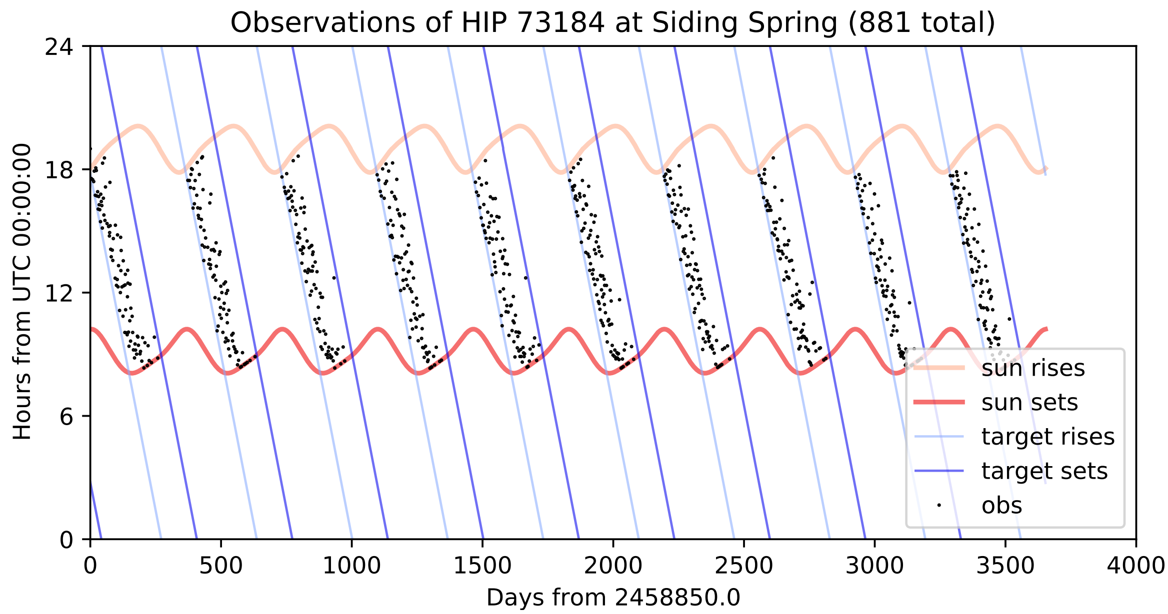

Figure 6. Observations of HIP 73184 (HD 131977) in the the architecture I simulation at Siding Spring Observatory. Local sunrise/set, star rise/set, and observation times for each day are shown.

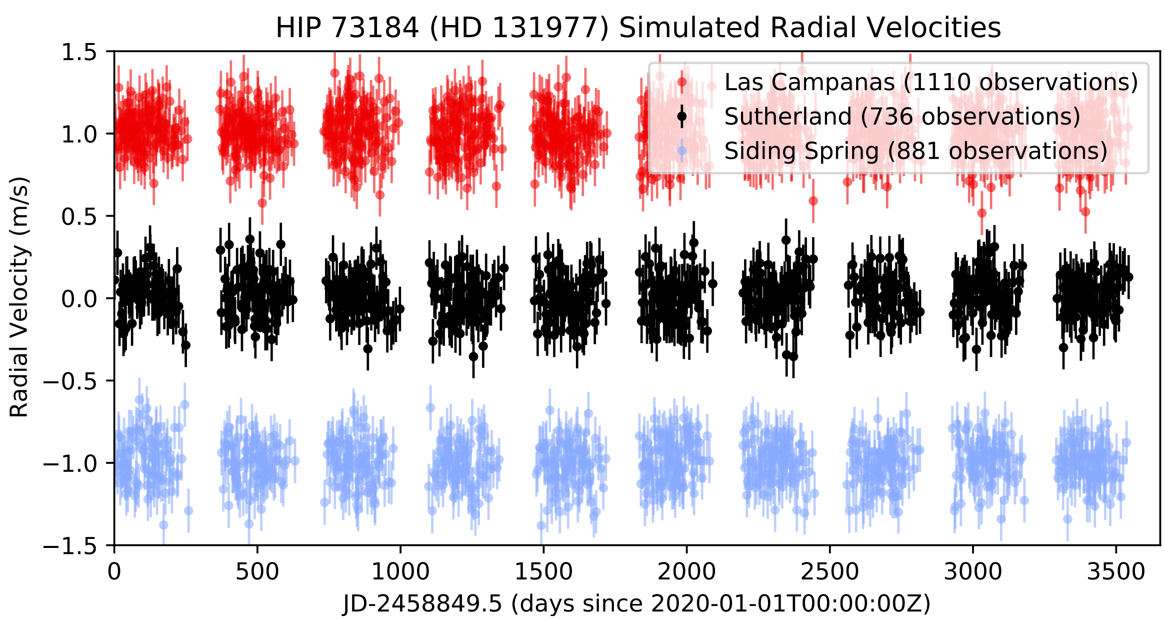

Figure 7. Simulated RV time-series for HIP 73184 (HD 131977) for Architecture I as observed by the three telescopes in its hemisphere (one each at Las Campanas, Sutherland, and Siding Spring). This star was chosen, as it has the median number of observations (2724) for the architecture. Note, only "white" noise is included in this simulation, despite the apparent correlated noise by eye during some seasons. The appearance of correlated noise could be partially due to the variable single measurement uncertainties from airmass extinction for a fixed exposure time over the course of a season.

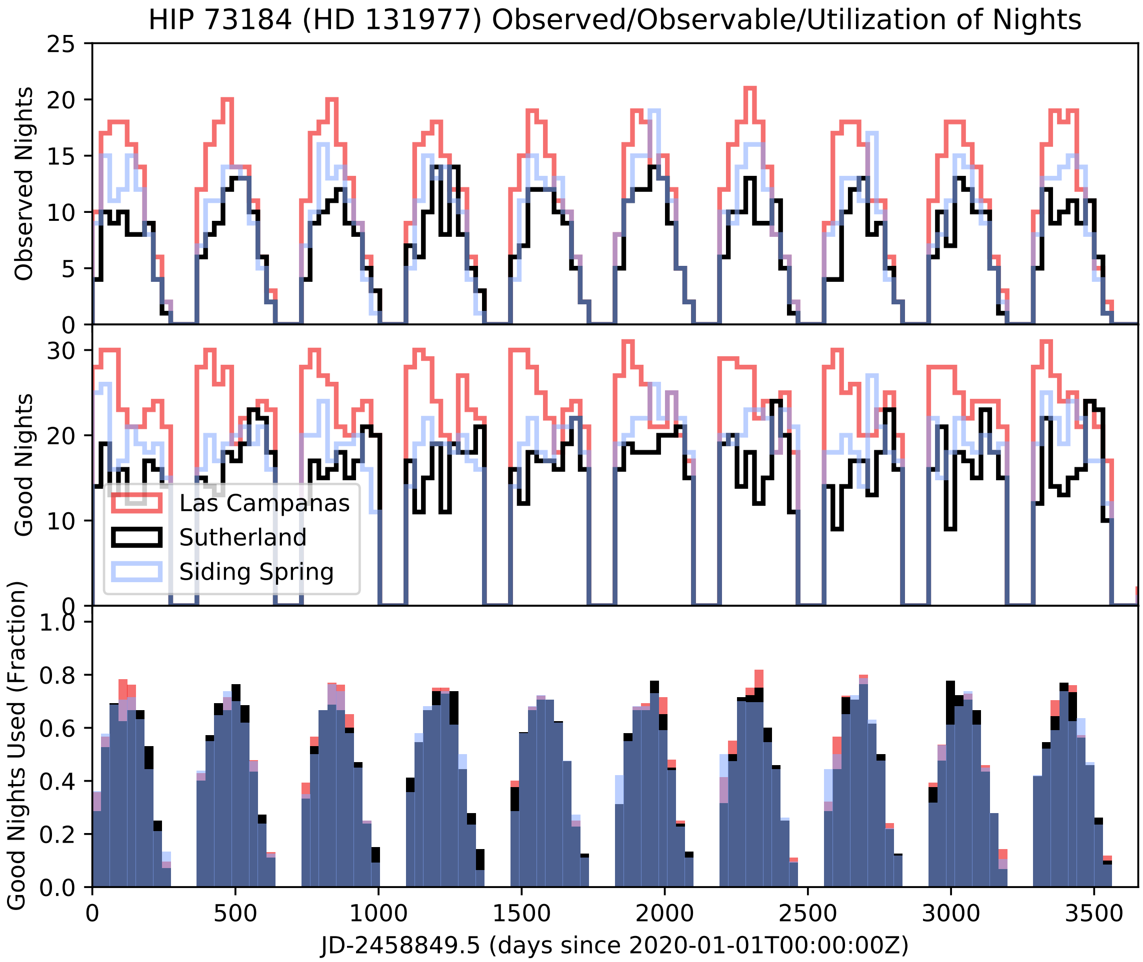

Figure 8. Simulated observation cadence and nightly availability for HIP 73184 (HD 131977) for Architecture I observed by three telescopes (one each at Las Campanas, Sutherland, and Siding Spring). Observations here are binned into 30.4375 day "months"; actual observations were never more than 1/night.

3. RESULTS: ARCHITECTURE EXPOSURE TIMES AND CADENCES

In this Section, we present summaries of the simulated radial velocity surveys for each of the architectures in turn. For each architecture, we present PDFs and CDFs of the stellar exposure times and number of observations of each star. These PDFs and CDFs are presented both for each telescope individually, and for certain combinations of telescopes within a given architecture. The 2/4/6 telescope combinations use the same number of telescopes in each hemisphere (1, 2, or 3), and we select the "best" ones first, e.g. those with the highest number of observations per star due to the different weather statistics. The best two sites are Mauna Kea and Las Campanas, then Kitt Peak and Sutherland, then Calar Alto and Siding Spring based upon the assumed weather statistics in Figure 5. This appeared to be consistent across all simulations of all architectures.

Second, we include PDFs and CDFs of the fraction of observable days during which each target star was observed. We bin by Julian date as opposed to the local "night", which varies for each site in the global network. Third, we compute and present theoretically optimal estimates of the achievable SNR for the detection of a K = 0.1 m/s planet, and the corresponding theoretical minimum detectable velocity semi-amplitude (for an SNR = 10) of a planet as per Equation 1. These estimates follow the idealized circular orbit and uniform cadence as described in §1, with the photon noise and instrument noise added in quadrature for the σ term. Future injection and recovery tests, combined with stellar activity models, could explore the impact our realistic cadences have on survey sensitivity. Finally, for all of the above, we compute summary statistics for the distribution of these values within an architecture (e.g. median, quartiles, 5^{th} and 95^{th} percentiles), which we use for the overall comparisons of the performance across all architectures in §4.

3.1. *Architecture I*

The subsections that follow have the same structure as presented here for Architecture I. We present six summary figures of PDFs (left-hand side) and six summary figures of CDFs (right-hand side) in the following order from top to bottom:

1. (Row 1) observations per star per telescope site;
2. Observations per star for combinations of telescope sites within the architecture;
3. Exposure times per star per telescope site;
4. Fraction of nights where a star that could be observed is observed for combinations of telescopes;
5. Theoretical minimum detectable semi-amplitude for a planet on a circular orbit (SNR of 10, Eqn 1 for homogeneous architectures or Eqn 2 in Section 3.6 for heterogeneous survey architectures) per telescope combination;
6. Maximum SNR of a planet detection for 10 cm/s semi-amplitude using the same theoretical approximation.

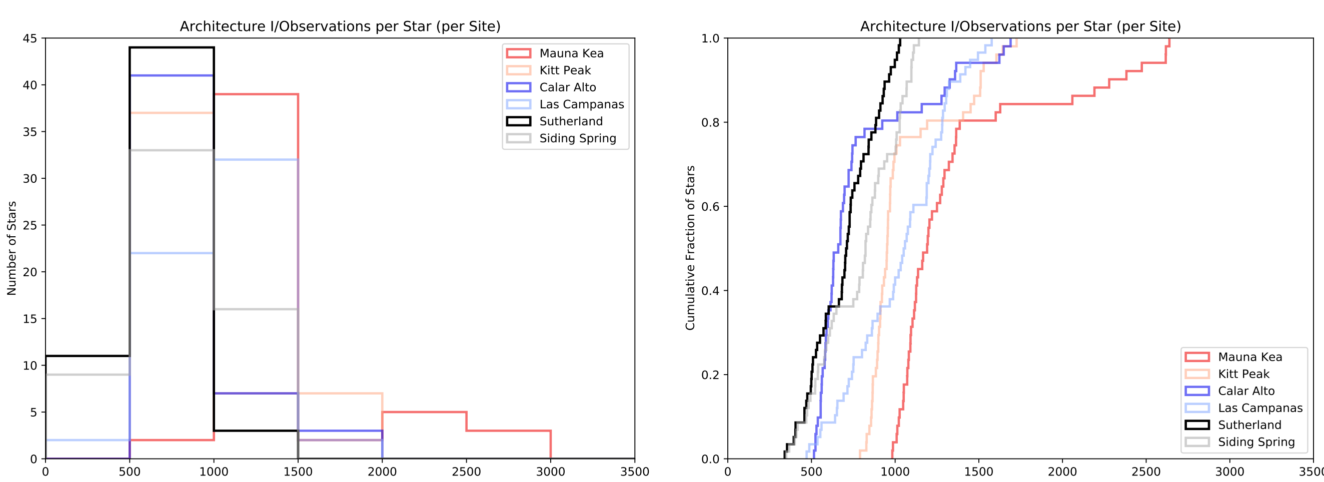

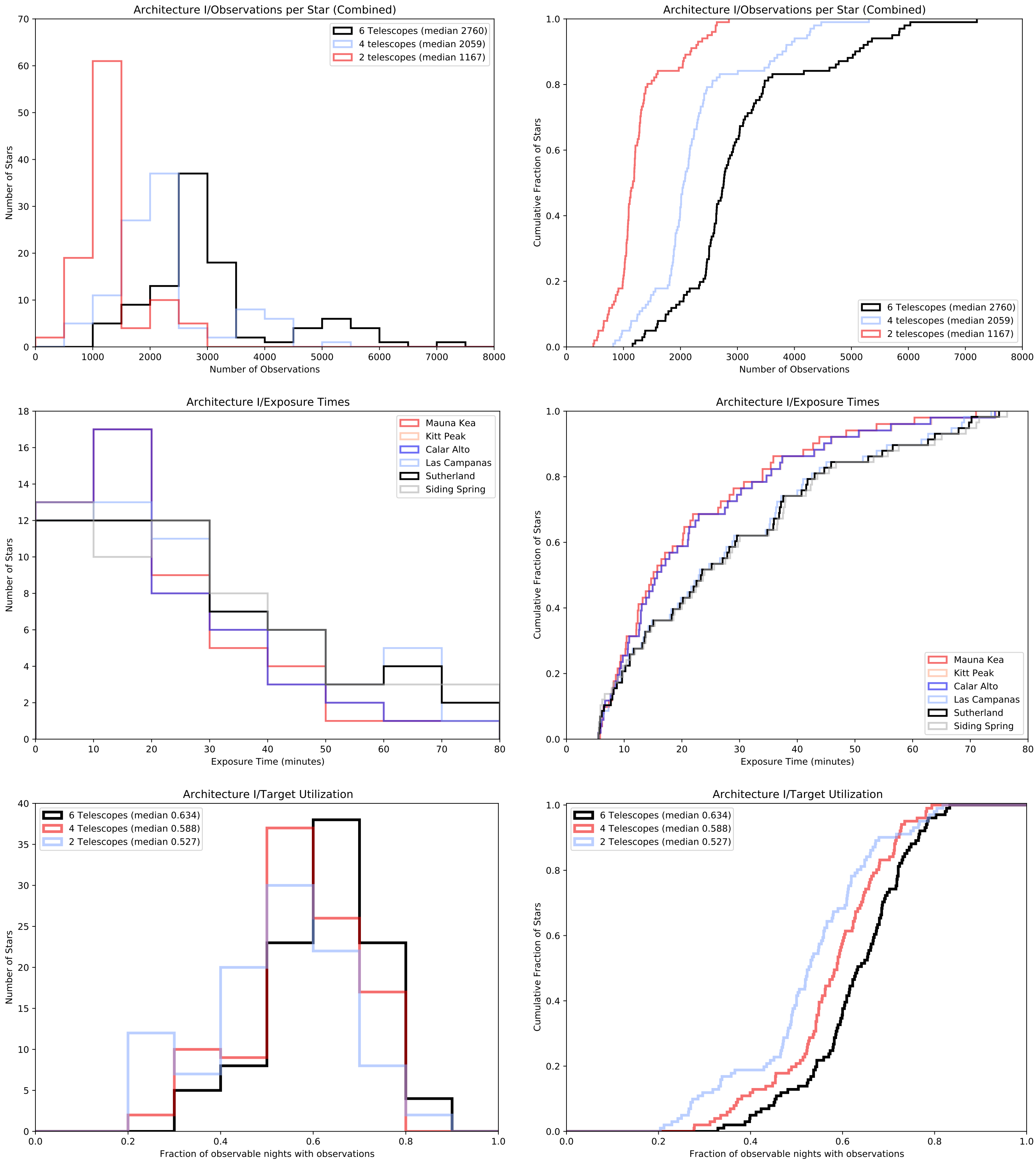
Architecture I/Observations per Star (Combined)
Number of Stars
Number of Observations
6 Telescopes (median 2760)
4 telescopes (median 2059)
2 telescopes (median 1167)
Architecture I/Observations per Star (Combined)
Cumulative Fraction of Stars
Number of Observations
6 Telescopes (median 2760)
4 telescopes (median 2059)
2 telescopes (median 1167)
Architecture I/Exposure Times
Number of Stars
Exposure Time (minutes)
Mauna Kea
Kitt Peak
Calar Alto
Las Campanas
Sutherland
Siding Spring
Architecture I/Exposure Times
Cumulative Fraction of Stars
Exposure Time (minutes)
Mauna Kea
Kitt Peak
Calar Alto
Las Campanas
Sutherland
Siding Spring
Architecture I/Target Utilization
Number of Stars
Fraction of observable nights with observations
6 Telescopes (median 0.634)
4 Telescopes (median 0.588)
2 Telescopes (median 0.527)
Architecture I/Target Utilization
Cumulative Fraction of Stars
Fraction of observable nights with observations
6 Telescopes (median 0.634)
4 Telescopes (median 0.588)
2 Telescopes (median 0.527)

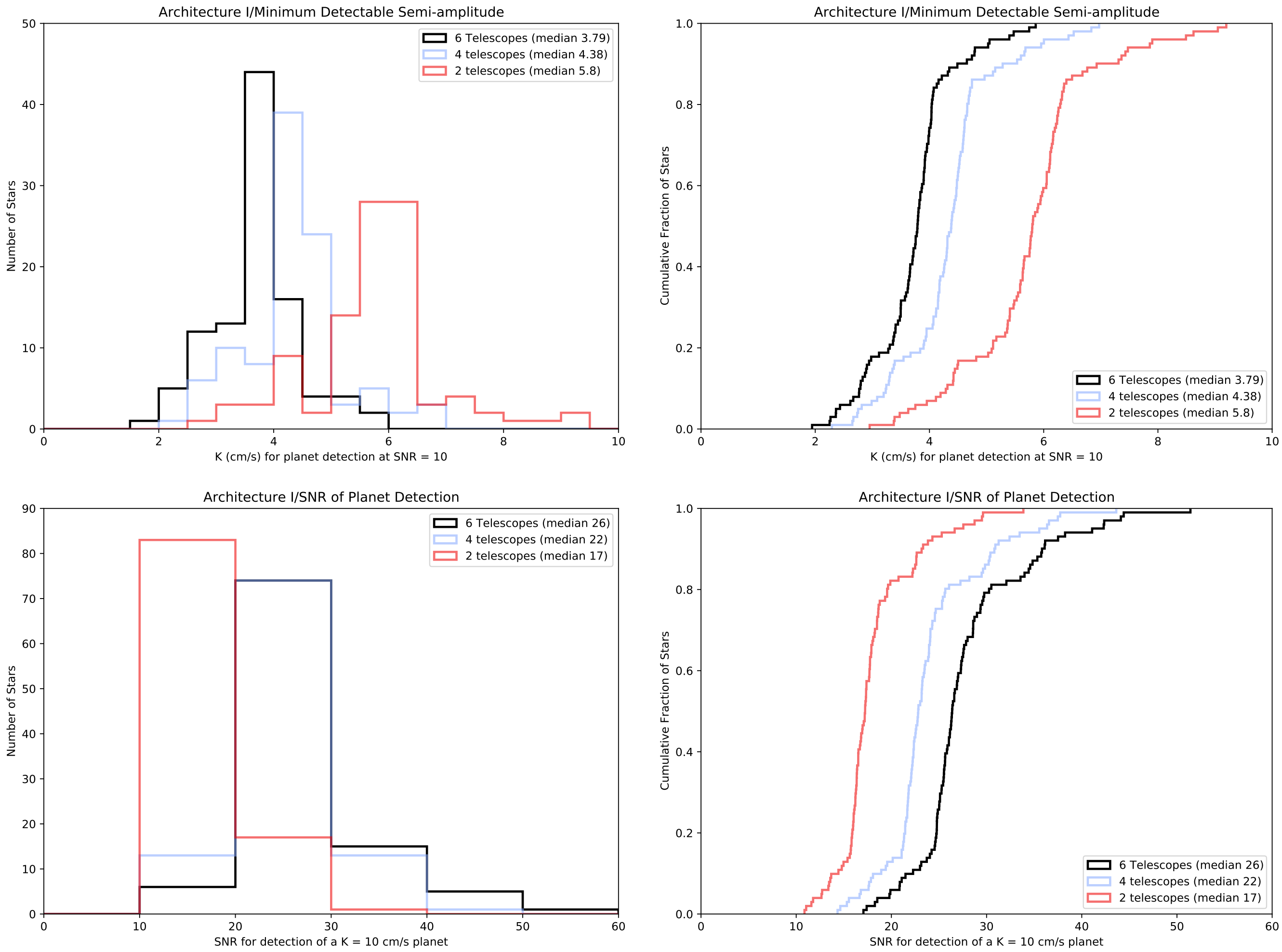
Architecture I/Minimum Detectable Semi-amplitude
6 Telescopes (median 3.79)
4 telescopes (median 4.38)
2 telescopes (median 5.8)
Number of Stars
K (cm/s) for planet detection at SNR = 10
Architecture I/Minimum Detectable Semi-amplitude
Cumulative Fraction of Stars
6 Telescopes (median 3.79)
4 telescopes (median 4.38)
2 telescopes (median 5.8)
K (cm/s) for planet detection at SNR = 10
Architecture I/SNR of Planet Detection
6 Telescopes (median 26)
4 telescopes (median 22)
2 telescopes (median 17)
Number of Stars
SNR for detection of a K = 10 cm/s planet
Architecture I/SNR of Planet Detection
Cumulative Fraction of Stars
6 Telescopes (median 26)
4 telescopes (median 22)
2 telescopes (median 17)
SNR for detection of a K = 10 cm/s planet

3.2. *Architecture IIa*

For this architecture, we simulate the 6-m telescopes at Mauna Kea and Las Campanas. For the 4-m telescopes, we re-use the simulations from architecture IIb; hence the identical PDFs and CDFs.

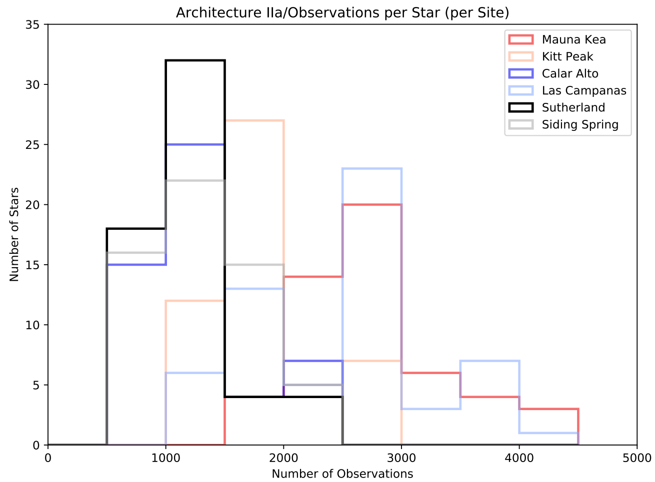

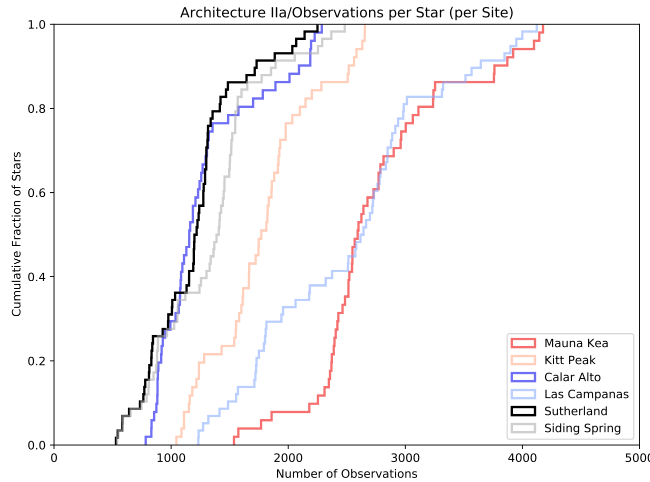

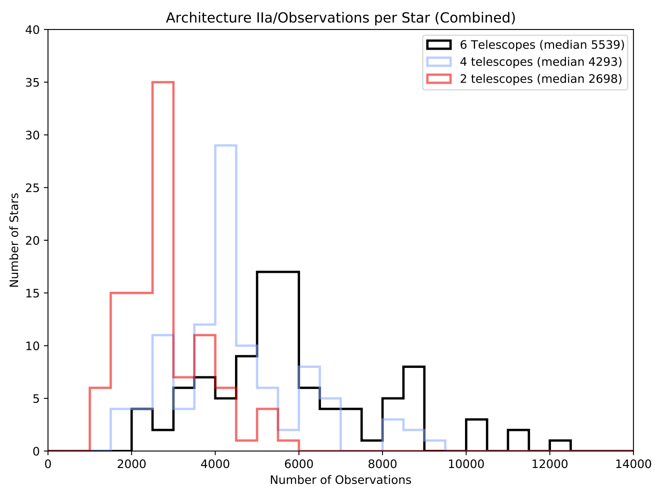

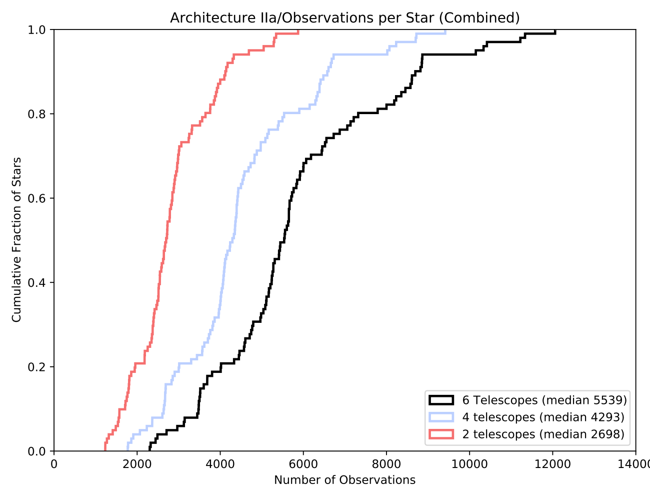

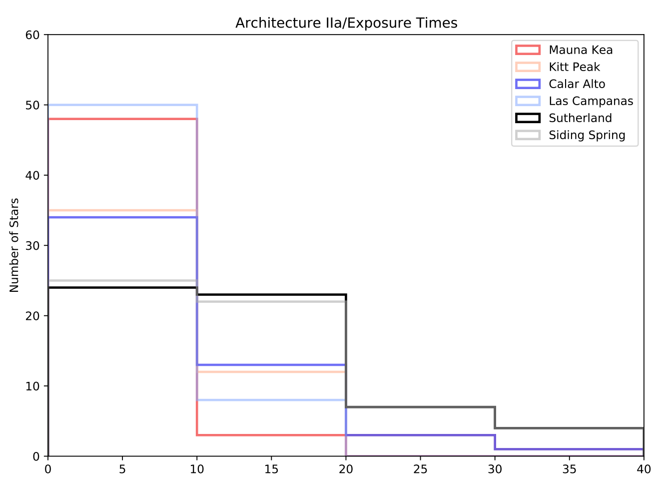

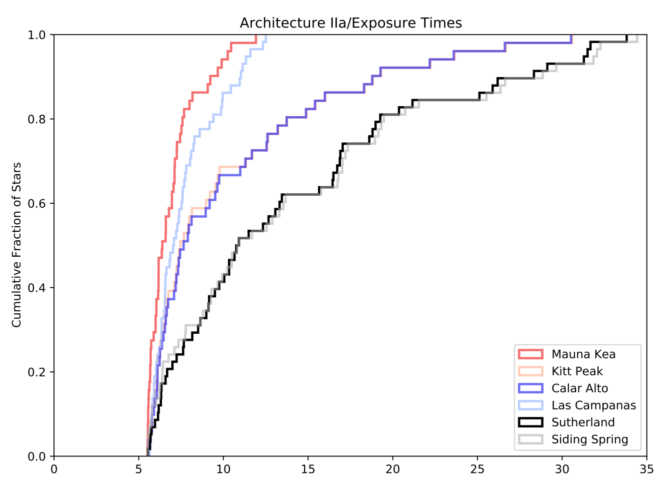

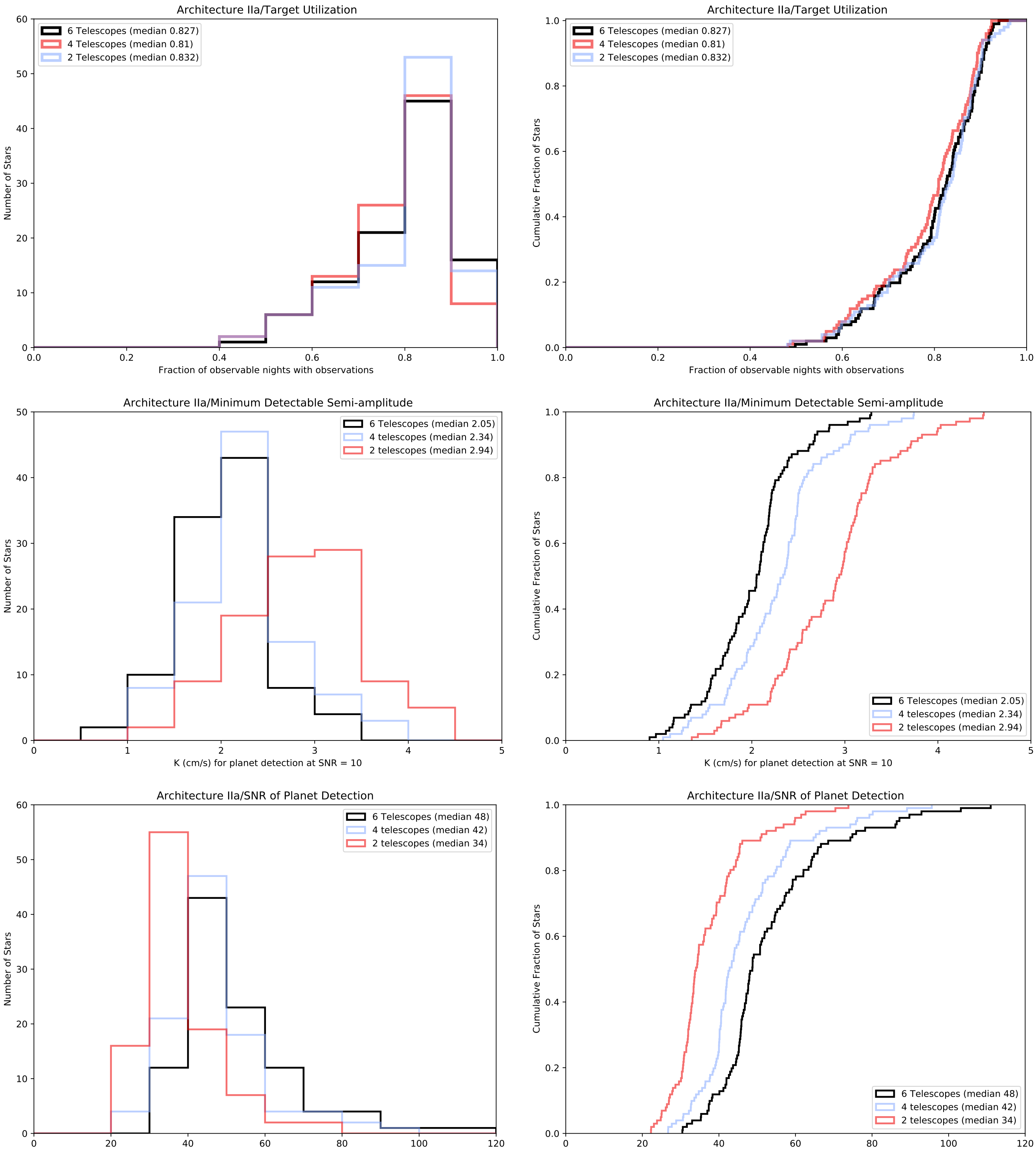
Architecture IIa/Target Utilization
6 Telescopes (median 0.827)
4 Telescopes (median 0.81)
2 Telescopes (median 0.832)
Number of Stars
Cumulative Fraction of Stars
Fraction of observable nights with observations
Architecture IIa/Minimum Detectable Semi-amplitude
6 Telescopes (median 2.05)
4 telescopes (median 2.34)
2 telescopes (median 2.94)
K (cm/s) for planet detection at SNR = 10
Architecture IIa/SNR of Planet Detection
6 Telescopes (median 48)
4 telescopes (median 42)
2 telescopes (median 34)
SNR for detection of a K = 10 cm/s planet

3.3. *Architecture IIb*

For this architecture, we simulate all six telescope locations. The telescope/instrument configurations at Kitt Peak, Calar Alto, Sutherland, and Siding Spring are then re-used in architecture IIa.

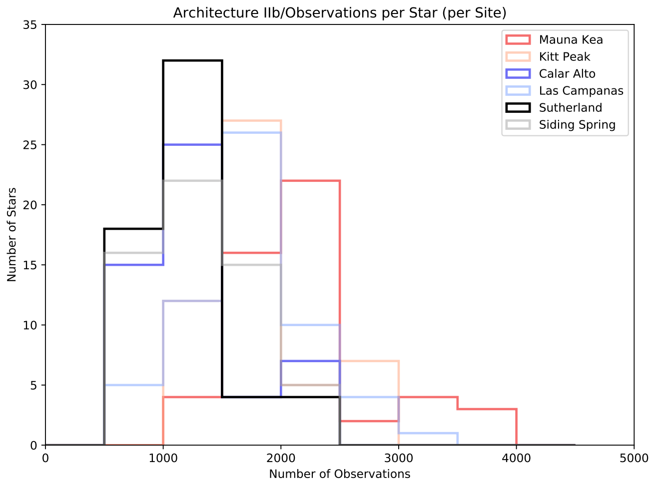

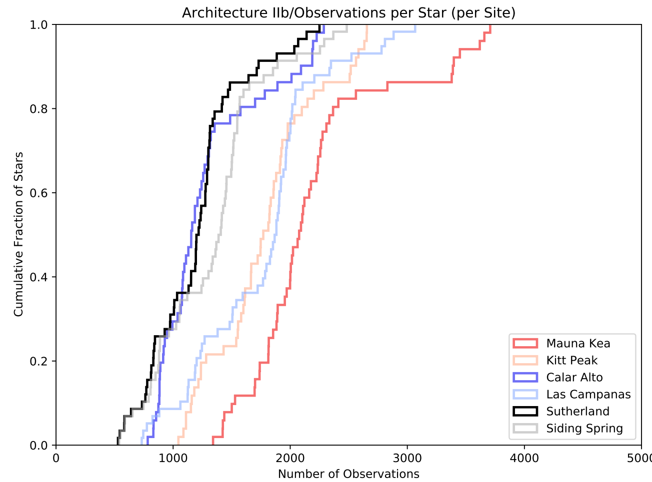

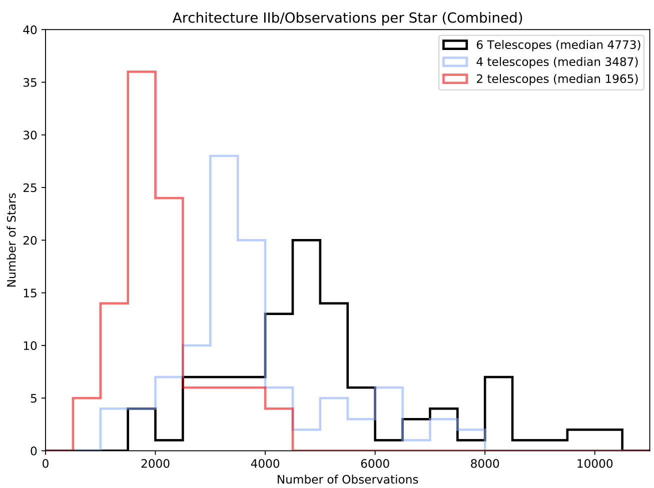

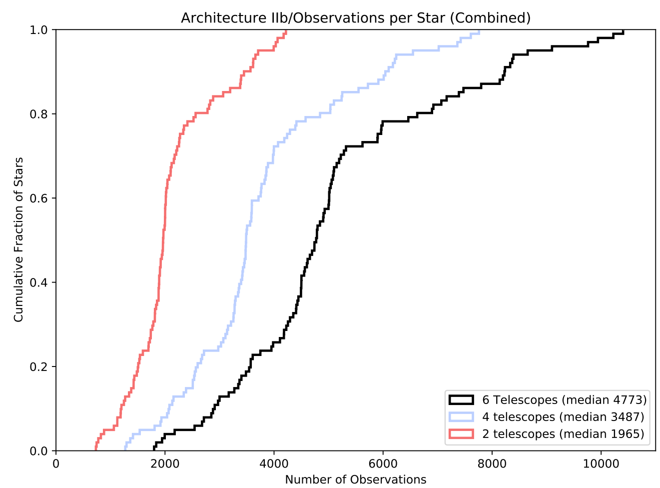

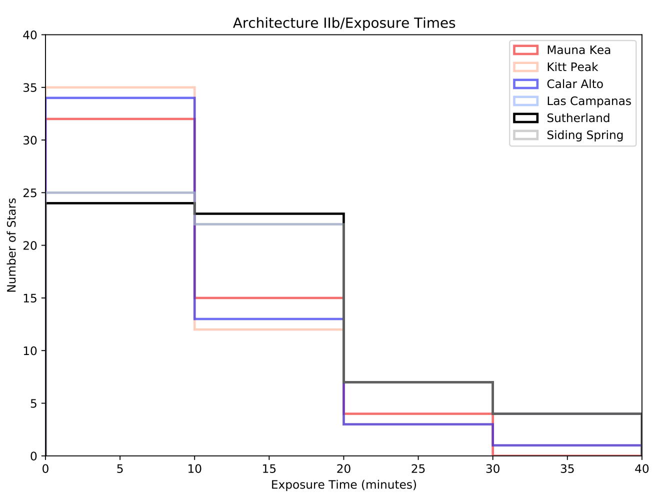

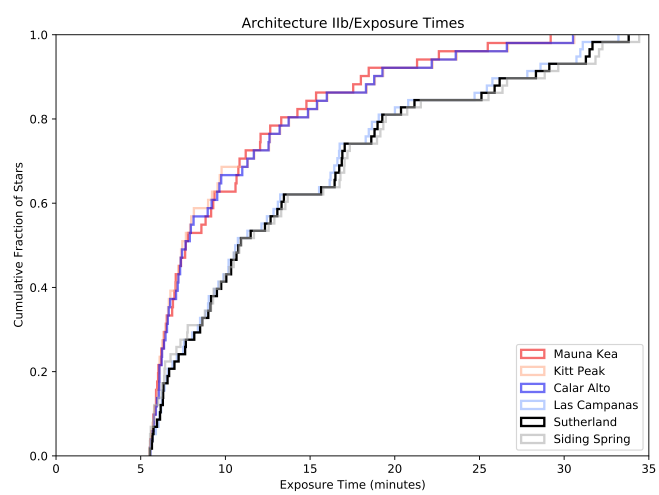

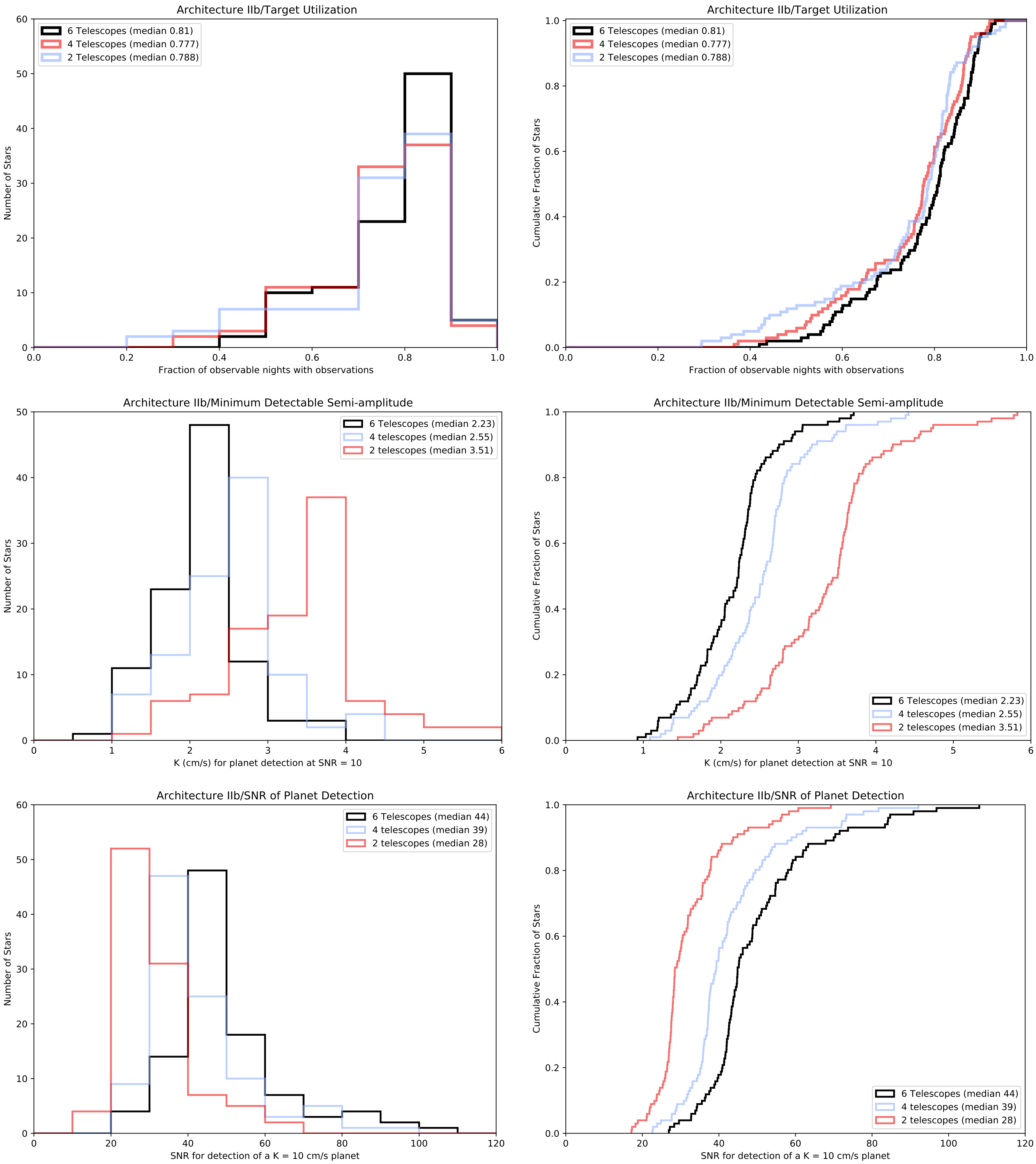
Architecture IIb/Target Utilization
6 Telescopes (median 0.81)
4 Telescopes (median 0.777)
2 Telescopes (median 0.788)
Number of Stars
Fraction of observable nights with observations
Architecture IIb/Target Utilization
6 Telescopes (median 0.81)
4 Telescopes (median 0.777)
2 Telescopes (median 0.788)
Cumulative Fraction of Stars
Fraction of observable nights with observations
Architecture IIb/Minimum Detectable Semi-amplitude
6 Telescopes (median 2.23)
4 telescopes (median 2.55)
2 telescopes (median 3.51)
Number of Stars
K (cm/s) for planet detection at SNR = 10
Architecture IIb/Minimum Detectable Semi-amplitude
6 Telescopes (median 2.23)
4 telescopes (median 2.55)
2 telescopes (median 3.51)
Cumulative Fraction of Stars
K (cm/s) for planet detection at SNR = 10
Architecture IIb/SNR of Planet Detection
6 Telescopes (median 44)
4 telescopes (median 39)
2 telescopes (median 28)
Number of Stars
SNR for detection of a K = 10 cm/s planet
Architecture IIb/SNR of Planet Detection
6 Telescopes (median 44)
4 telescopes (median 39)
2 telescopes (median 28)
Cumulative Fraction of Stars
SNR for detection of a K = 10 cm/s planet

3.4. *Architecture V*

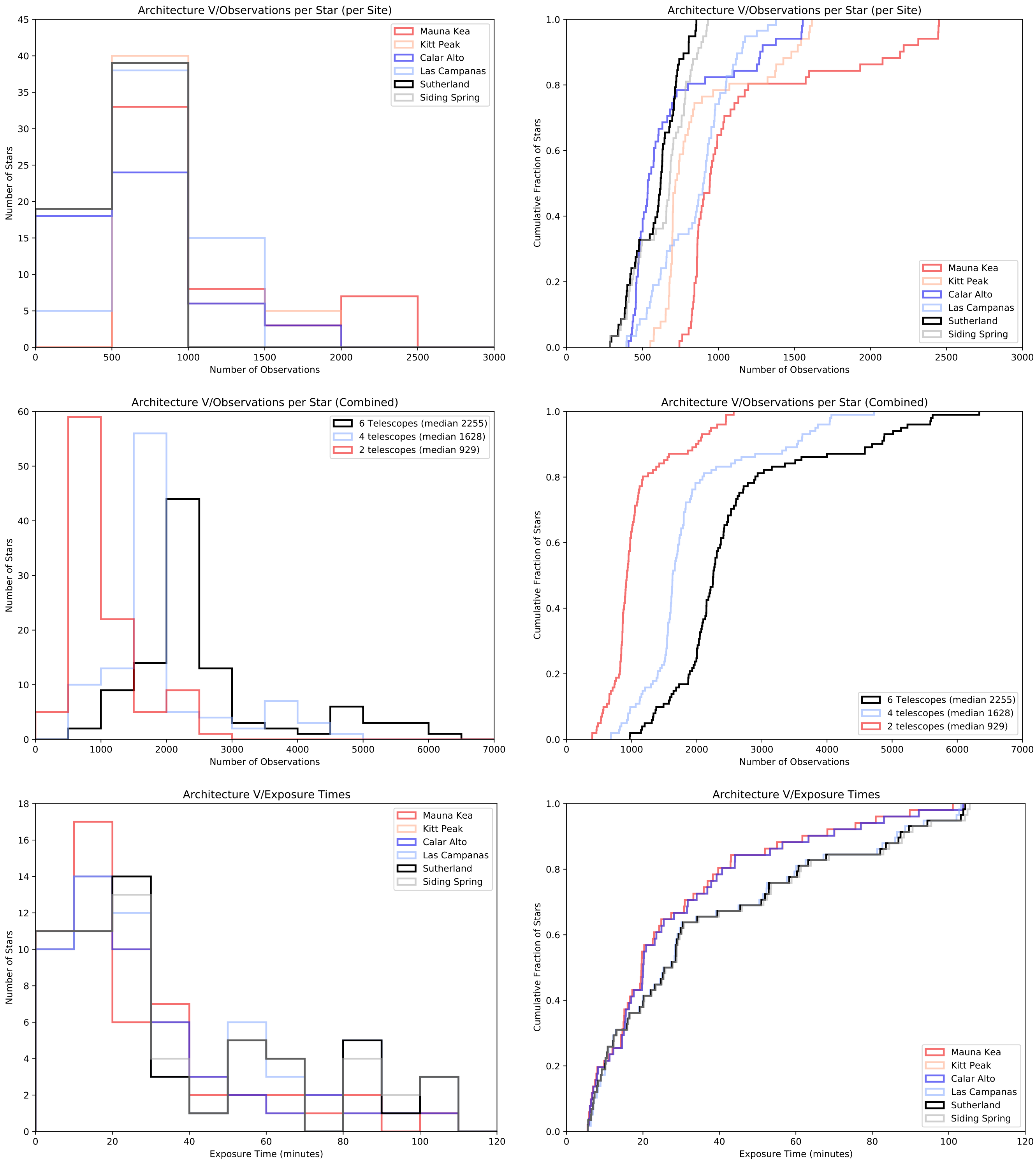

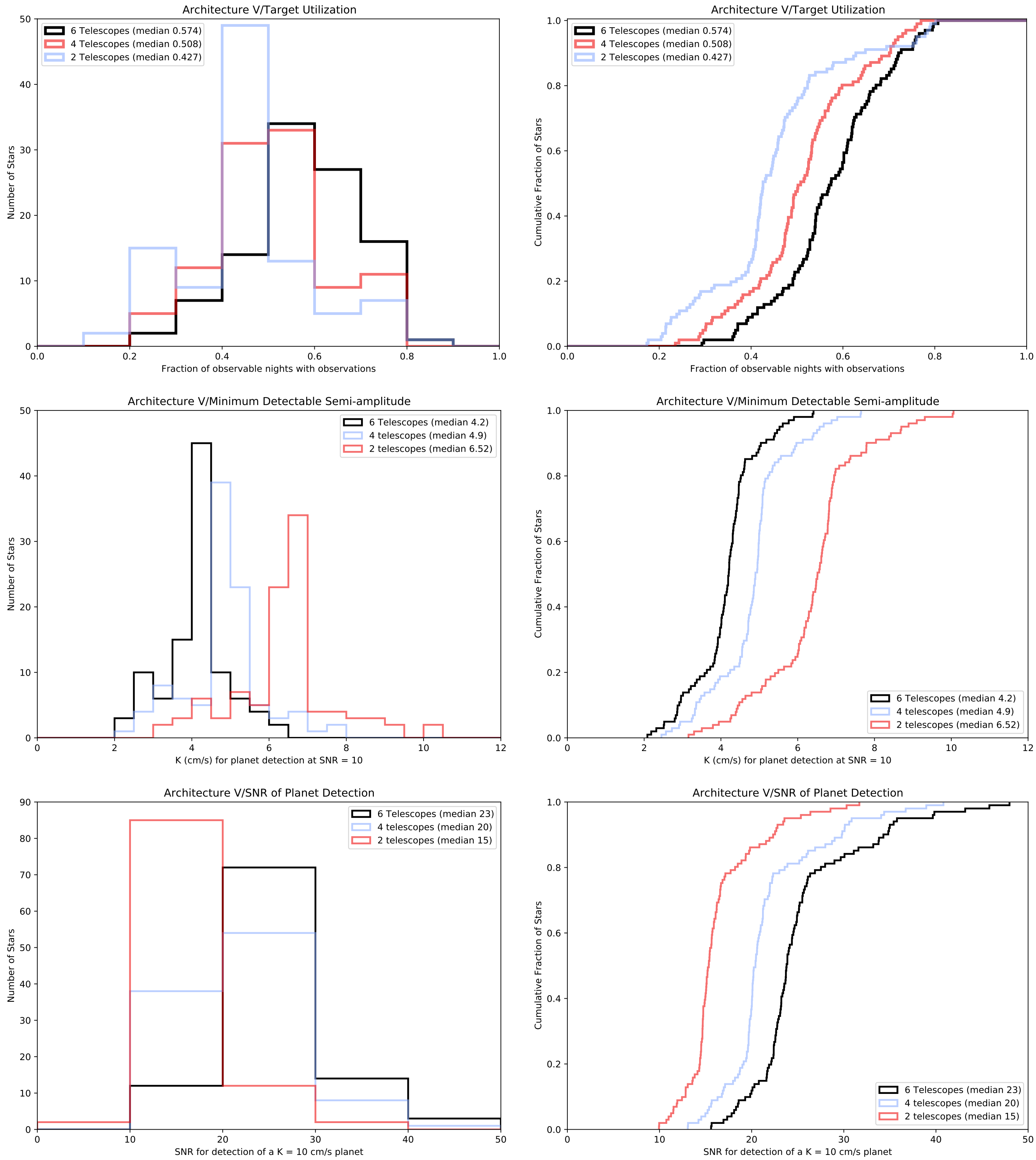

Architecture V/Target Utilization
6 Telescopes (median 0.574)
4 Telescopes (median 0.508)
2 Telescopes (median 0.427)
Number of Stars
Cumulative Fraction of Stars
Fraction of observable nights with observations
Architecture V/Minimum Detectable Semi-amplitude
6 Telescopes (median 4.2)
4 telescopes (median 4.9)
2 telescopes (median 6.52)
K (cm/s) for planet detection at SNR = 10
Architecture V/SNR of Planet Detection
6 Telescopes (median 23)
4 telescopes (median 20)
2 telescopes (median 15)
SNR for detection of a K = 10 cm/s planet

3.5. *Architecture VI*

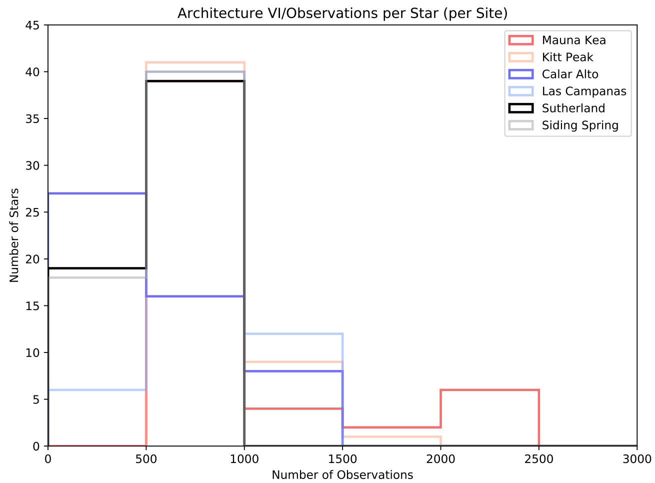

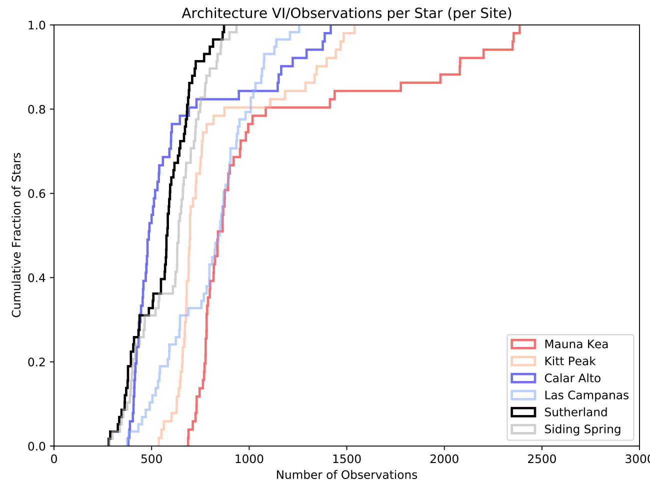

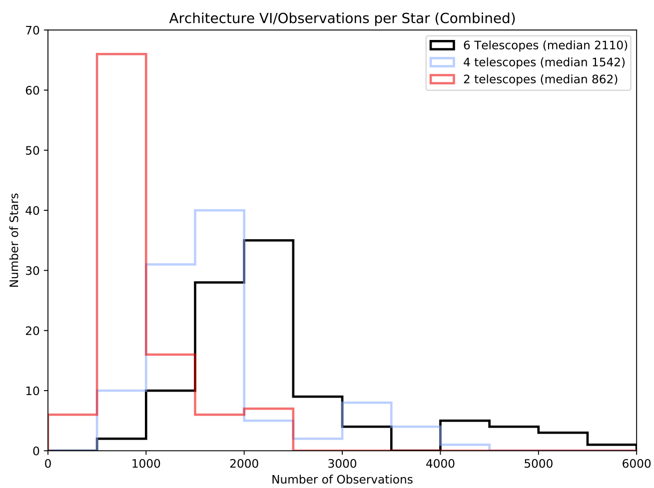

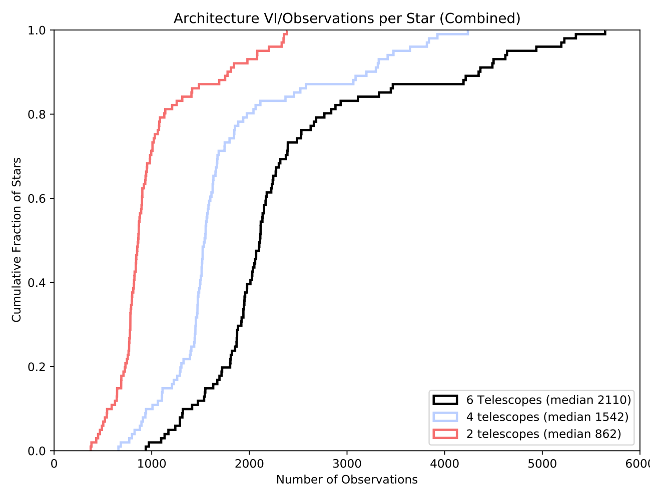

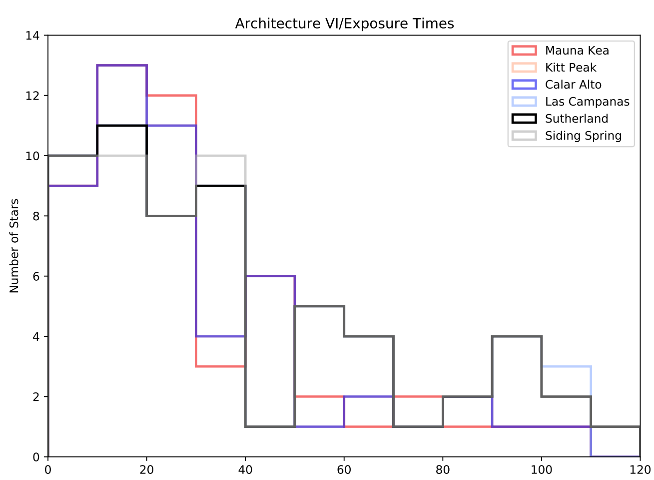

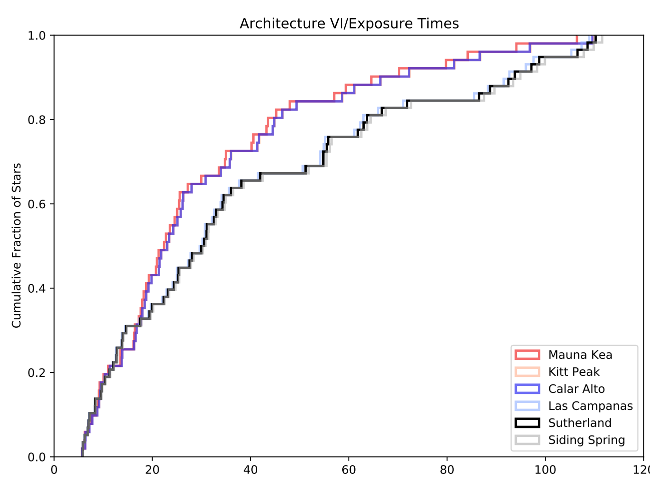

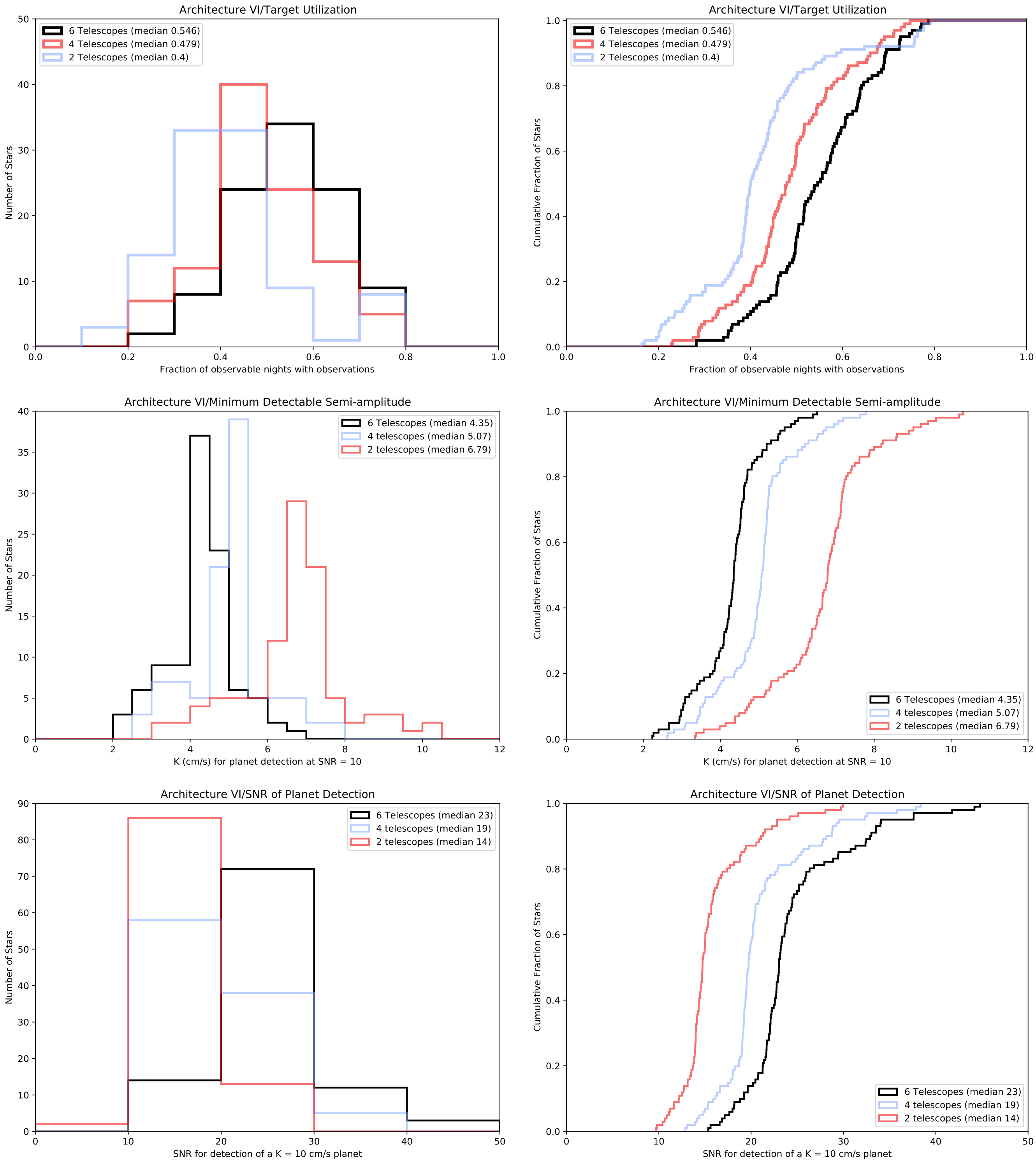
Architecture VI/Target Utilization
6 Telescopes (median 0.546)
4 Telescopes (median 0.479)
2 Telescopes (median 0.4)
Number of Stars
Fraction of observable nights with observations
Architecture VI/Target Utilization
6 Telescopes (median 0.546)
4 Telescopes (median 0.479)
2 Telescopes (median 0.4)
Cumulative Fraction of Stars
Fraction of observable nights with observations
Architecture VI/Minimum Detectable Semi-amplitude
6 Telescopes (median 4.35)
4 telescopes (median 5.07)
2 telescopes (median 6.79)
Number of Stars
K (cm/s) for planet detection at SNR = 10
Architecture VI/Minimum Detectable Semi-amplitude
6 Telescopes (median 4.35)
4 telescopes (median 5.07)
2 telescopes (median 6.79)
Cumulative Fraction of Stars
K (cm/s) for planet detection at SNR = 10
Architecture VI/SNR of Planet Detection
6 Telescopes (median 23)
4 telescopes (median 19)
2 telescopes (median 14)
Number of Stars
SNR for detection of a K = 10 cm/s planet
Architecture VI/SNR of Planet Detection
6 Telescopes (median 23)
4 telescopes (median 19)
2 telescopes (median 14)
Cumulative Fraction of Stars
SNR for detection of a K = 10 cm/s planet

3.6. *Architecture VIIIa*

For this architecture, not all combinations of large and small telescopes are shown. In particular, the 2 and 4 small telescope cases (with and without large telescopes) are not shown to reduce clutter.

The higher RV precision requirements of the 10-m telescopes result in fairly similar exposure times compared to the 3.5-m apertures with lower RV precision requirements. Consequently, the 10-m apertures have a similar number of observations per star per usable night, despite the larger apertures. However, given the smaller time allocation available on the 10-m apertures, this results in an overall lower number of observations per star for those telescopes. The noise distributions are different for different telescopes in this architecture, so we derive a two-precision theoretical SNR equation, expanded from 1 to be:

$$SNR = K\sqrt{\frac{1}{2}\left(\frac{N_{\text{obs1}}}{2\sigma_1^2} + \frac{N_{\text{obs2}}}{2\sigma_2^2}\right)} \tag{2}$$

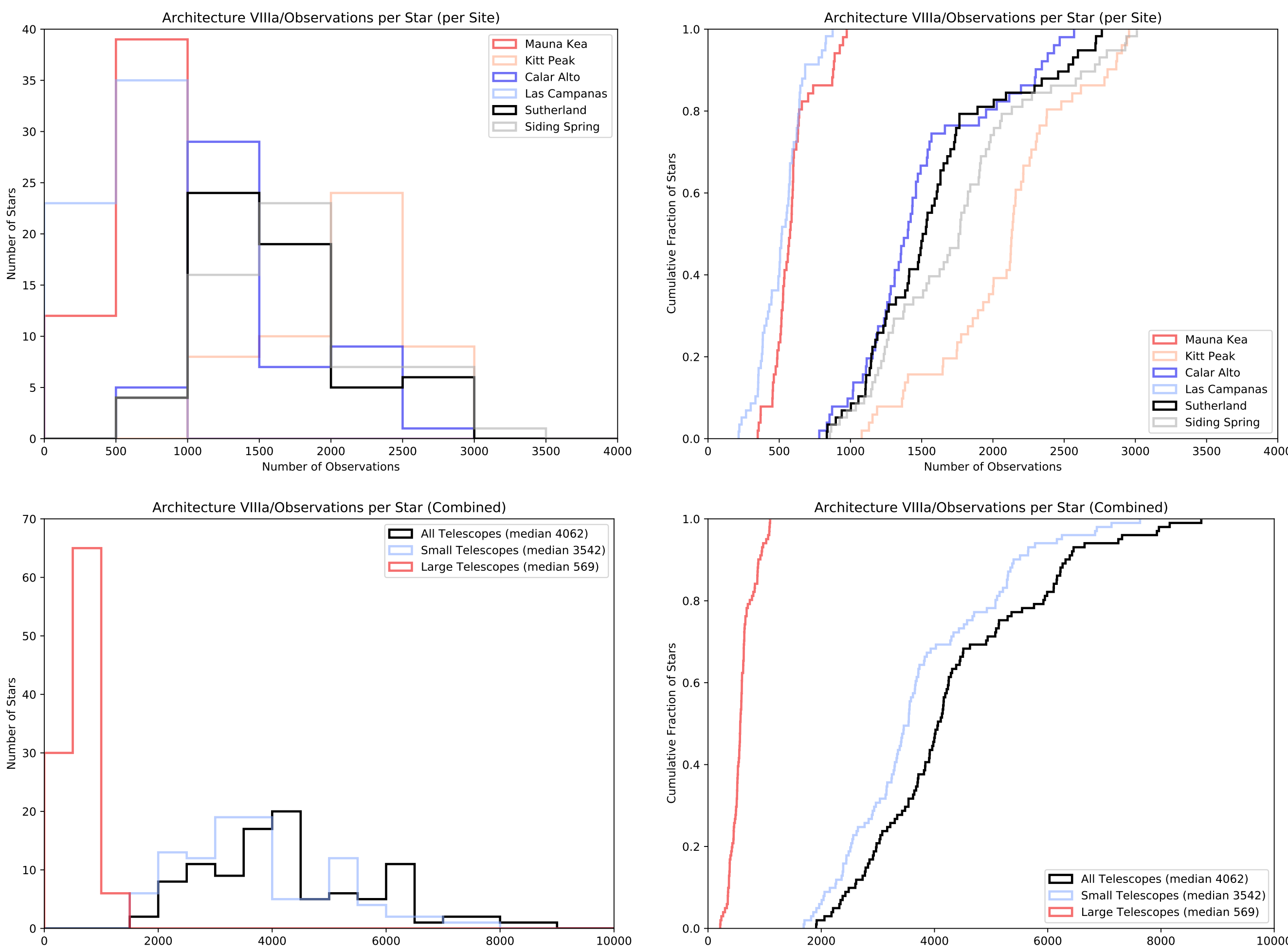

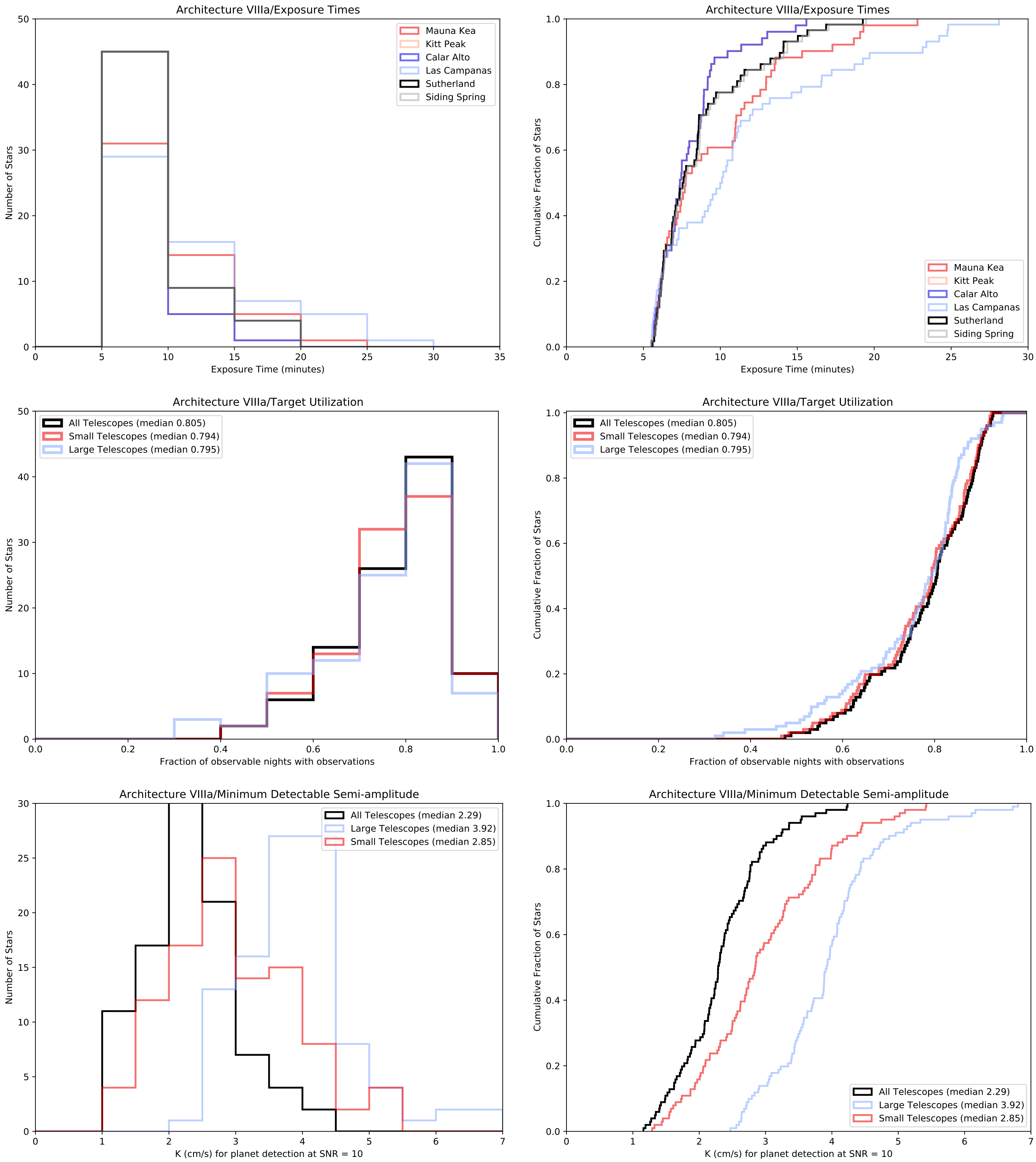
Architecture VIIIa/Exposure Times
Number of Stars
Exposure Time (minutes)
Mauna Kea
Kitt Peak
Calar Alto
Las Campanas
Sutherland
Siding Spring
Architecture VIIIa/Exposure Times
Cumulative Fraction of Stars
Exposure Time (minutes)
Mauna Kea
Kitt Peak
Calar Alto
Las Campanas
Sutherland
Siding Spring
Architecture VIIIa/Target Utilization
Number of Stars
Fraction of observable nights with observations
All Telescopes (median 0.805)
Small Telescopes (median 0.794)
Large Telescopes (median 0.795)
Architecture VIIIa/Target Utilization
Cumulative Fraction of Stars
Fraction of observable nights with observations
All Telescopes (median 0.805)
Small Telescopes (median 0.794)
Large Telescopes (median 0.795)
Architecture VIIIa/Minimum Detectable Semi-amplitude
Number of Stars
K (cm/s) for planet detection at SNR = 10
All Telescopes (median 2.29)
Large Telescopes (median 3.92)
Small Telescopes (median 2.85)
Architecture VIIIa/Minimum Detectable Semi-amplitude
Cumulative Fraction of Stars
K (cm/s) for planet detection at SNR = 10
All Telescopes (median 2.29)
Large Telescopes (median 3.92)
Small Telescopes (median 2.85)

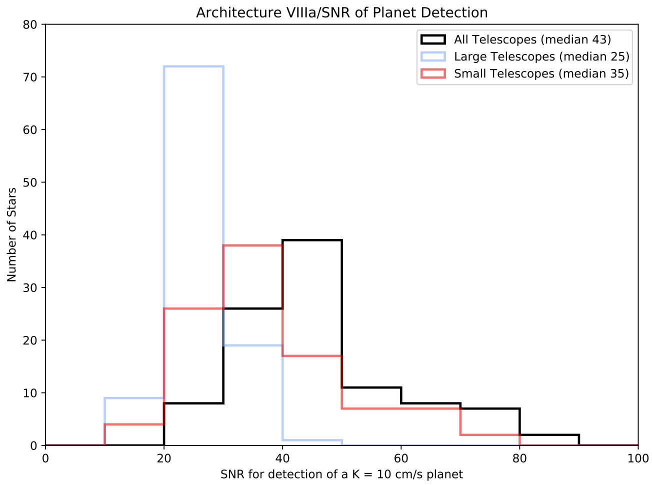
Architecture VIIIa/SNR of Planet Detection
All Telescopes (median 43)
Large Telescopes (median 25)
Small Telescopes (median 35)
Number of Stars
SNR for detection of a K = 10 cm/s planet

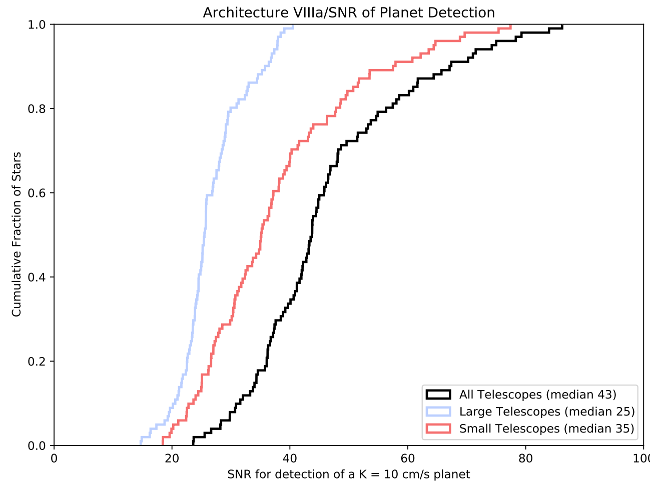
Architecture VIIIa/SNR of Planet Detection
All Telescopes (median 43)
Large Telescopes (median 25)
Small Telescopes (median 35)
Cumulative Fraction of Stars
SNR for detection of a K = 10 cm/s planet

3.7. *Architecture VIIIb*

This architecture is broadly similar to architecture VIIIa, though the small telescopes are six 2.4 m telescopes (comparable to architecture I), instead of four 3.5 m telescopes (comparable to architecture IIa). For legibility, in the plots that follow, only the small (2.4-m) telescopes are shown in the exposure time plots. The simulations of the 10-m telescopes from architecture VIIIa are reused here. Again as in architecture VIIIa, not all large/small telescope combinations are shown. Additionally, the detection calculations consider the differing instrument sensitivities using equation 2.

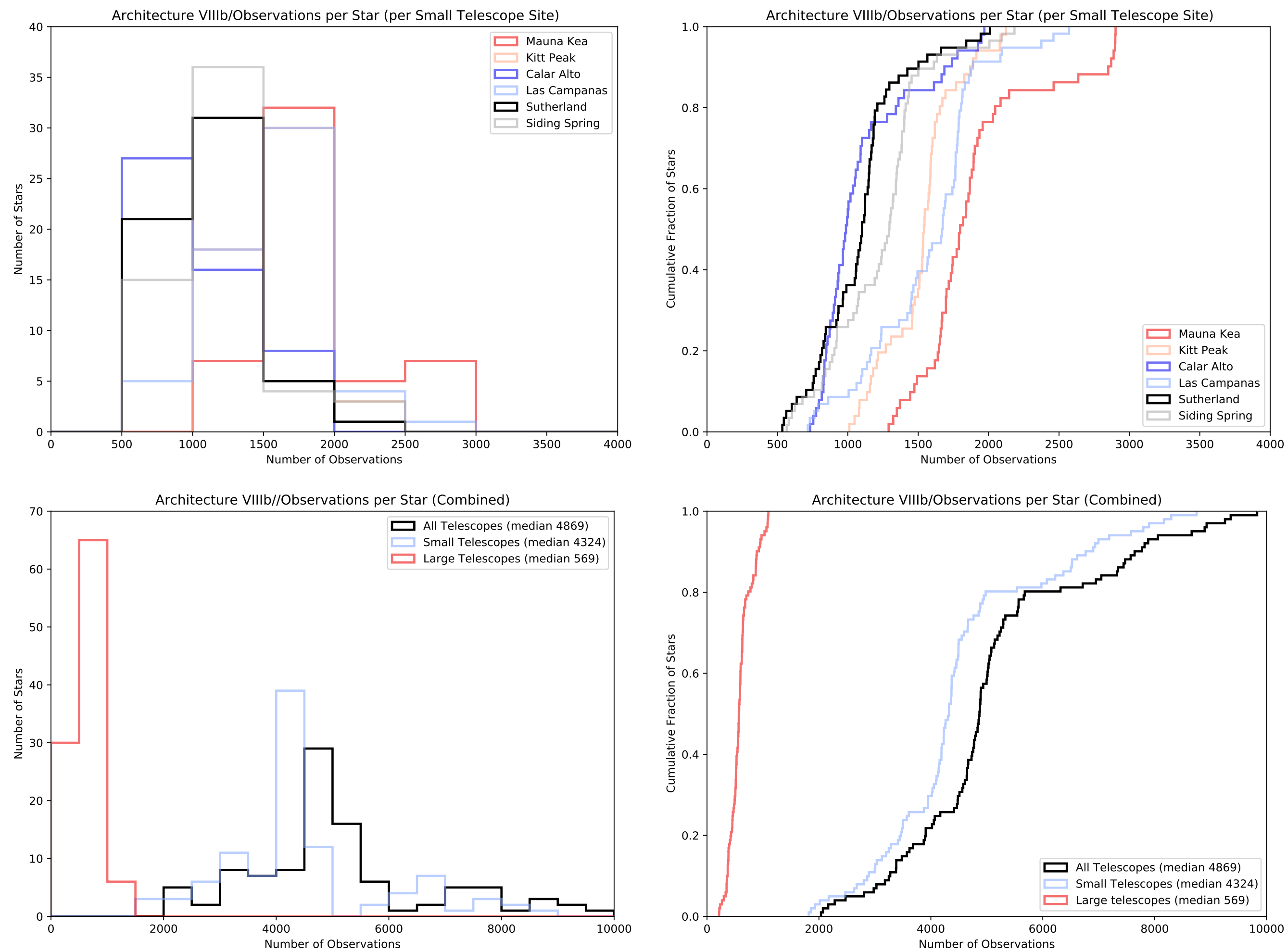

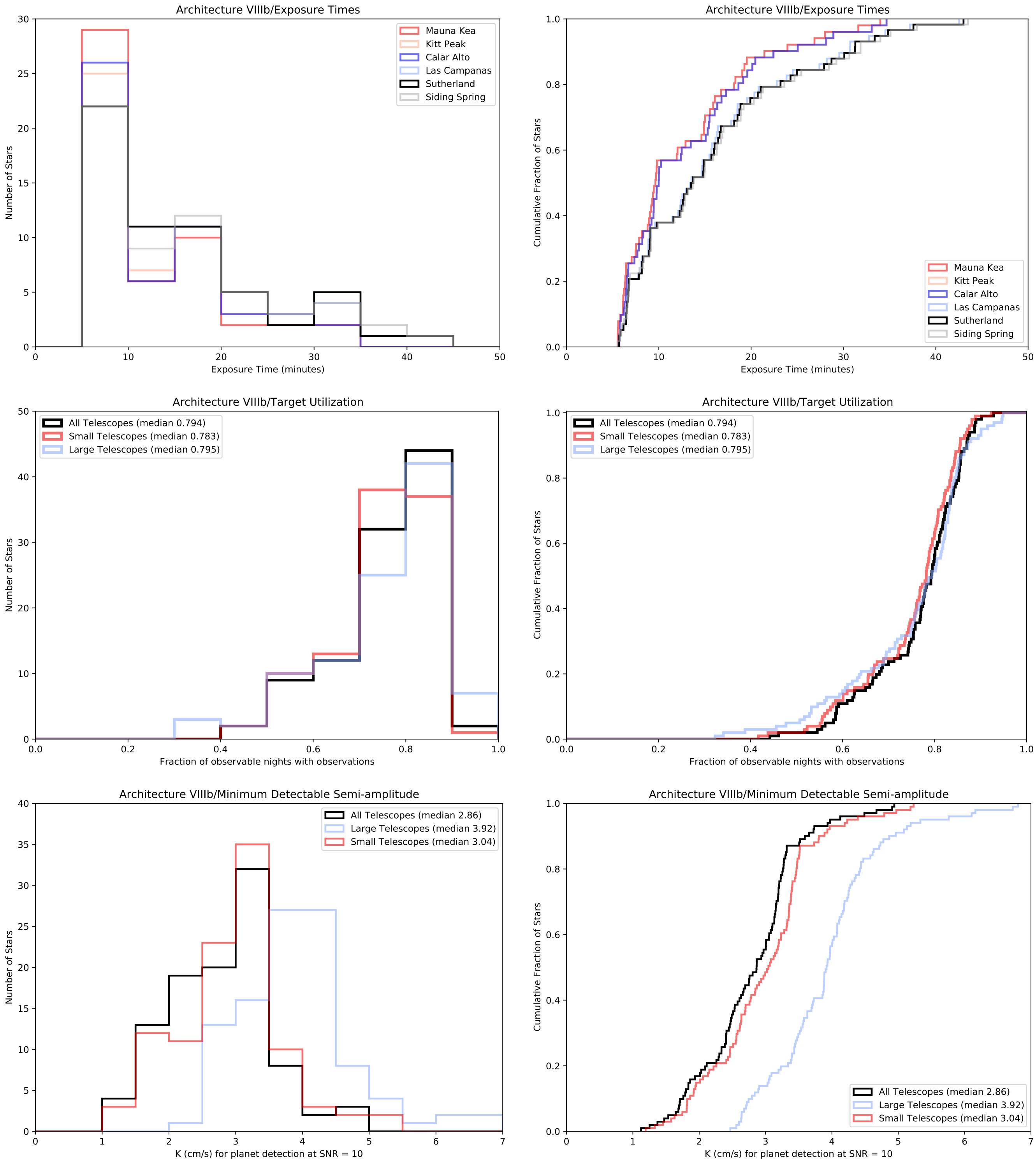

Architecture VIIIb/Exposure Times
Mauna Kea
Kitt Peak
Calar Alto
Las Campanas
Sutherland
Siding Spring
Number of Stars
Exposure Time (minutes)
Architecture VIIIb/Exposure Times
Cumulative Fraction of Stars
Exposure Time (minutes)
Architecture VIIIb/Target Utilization
All Telescopes (median 0.794)
Small Telescopes (median 0.783)
Large Telescopes (median 0.795)
Number of Stars
Fraction of observable nights with observations
Architecture VIIIb/Target Utilization
Cumulative Fraction of Stars
Fraction of observable nights with observations
Architecture VIIIb/Minimum Detectable Semi-amplitude
All Telescopes (median 2.86)
Large Telescopes (median 3.92)
Small Telescopes (median 3.04)
Number of Stars
K (cm/s) for planet detection at SNR = 10
Architecture VIIIb/Minimum Detectable Semi-amplitude
Cumulative Fraction of Stars
K (cm/s) for planet detection at SNR = 10

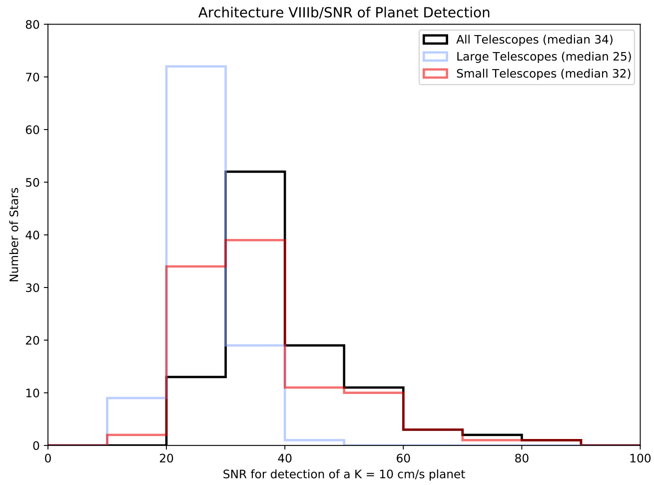
Architecture VIIIb/SNR of Planet Detection
All Telescopes (median 34)
Large Telescopes (median 25)
Small Telescopes (median 32)
Number of Stars
SNR for detection of a K = 10 cm/s planet

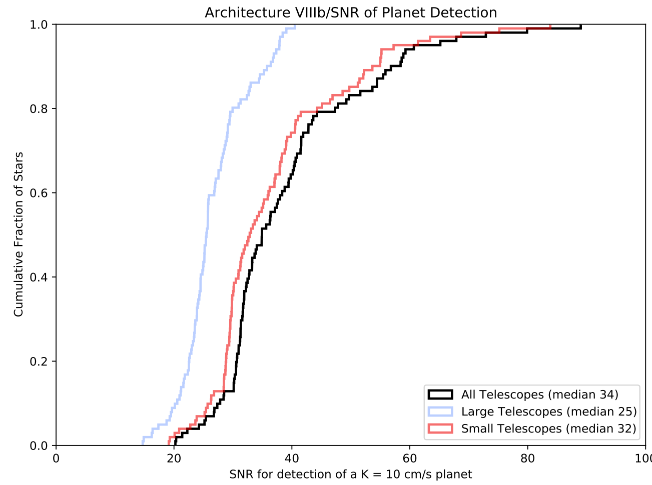
Architecture VIIIb/SNR of Planet Detection
Cumulative Fraction of Stars
All Telescopes (median 34)
Large Telescopes (median 25)
Small Telescopes (median 32)
SNR for detection of a K = 10 cm/s planet

4. RESULTS: ARCHITECTURE COMPARISON

In this section we present our key findings from a comparison between architectures in our survey simulations. First, we present a summary of the number of observations per star for each architecture, summed across all telescopes within an architecture (Figure 9). The baseline case with the baseline spectrometer can be considered as an (aperture × time allocation) figure of merit, while the others leverage particular defined spectrograph specifications and SNR and RV precision optimizations as specified.

Second, we present a cross-architecture summary of the fraction of observable days during which each target star was observed; we use the same binning procedure as in section 3. This figure of merit represents the effective achieved cadences of each architecture given the size of the target list. Third, we present a cross-architecture summary of the maximum (photon noise) SNR for the detection of a K = 0.1 m/s planet, and minimum (photon noise) detectable semi-amplitude for an SNR = 10 planet, per equations 1 and 2. This simple photon noise metric we have adopted represents a theoretical optimistic limit to what can be achieved in a real survey impacted by instrumental systematics, stellar activity, and other RV noise terms, but offers the most straightforward and direct means for assessing how the number of observations per star achieved for a given architecture maps to exoplanet sensitivity. The impacts of correlated noise on RV survey detection efficiency is the subject of follow-on work. Finally, in Figure 11 we show the median detectable semi-amplitude K and median SNR for a $K = 0.1$ m/s for each architecture. These are directly anti-correlated and correlated with the achieved number of observations per star for a given architecture in Figure 9, as might be expected.

From these figures of merit, we can reach several conclusions. First, we find that the minimum SNR per resolution element requirements did not significantly increase exposure times relative to the required photon noise single measurement precision. In other words, they were approximately equivalent requirements. Second, whether or not an architecture achieves nightly cadence is determined largely by the collective telescope aperture, as might be expected. In the case of architecture VIIIb, the differences in specified surveys RV photon noise precision and time allocation of the 10-m telescopes also had significant effects. All architectures come close to or slightly exceed achieving an effectively nightly cadence for the specified target list, but that requires three telescope per hemisphere in order to do so; e.g. the typical cadence for a single telescope site within an architecture does not achieve a nightly cadence by a factor of ∼3, given the assumptions, target list size, and this level of desired RV precision. Third, the differences in number of observations between sites in a given hemisphere correlates with number of clear nights, as might be expected. Future optimizations of a simulated RV survey could sculpt target lists and dynamically set priorities on a given telescope in a given hemisphere depending on the weather conditions at other sites.

Fourth, some stars are rarely observed for various reasons (right ascension, declination, and/or long exposure time), and they are least observed by telescopes with limited time allocation; e.g. the minimum outliers in the box-and-whiskers plots of Figures 9 and 10. In this case, adding more telescopes increased the fraction of observable nights used. A more complex target queue scheduling prioritization schema will be necessary for some targets, instead of the hour angle and time since last observation weighting simulated herein, in order to achieve a more uniform number of observations per star. By comparison, architectures that were “efficient” with short exposure times were able to observe almost every available star every night. In that case, adding more sites increased the number of observations, but not the fraction of observable nights used.

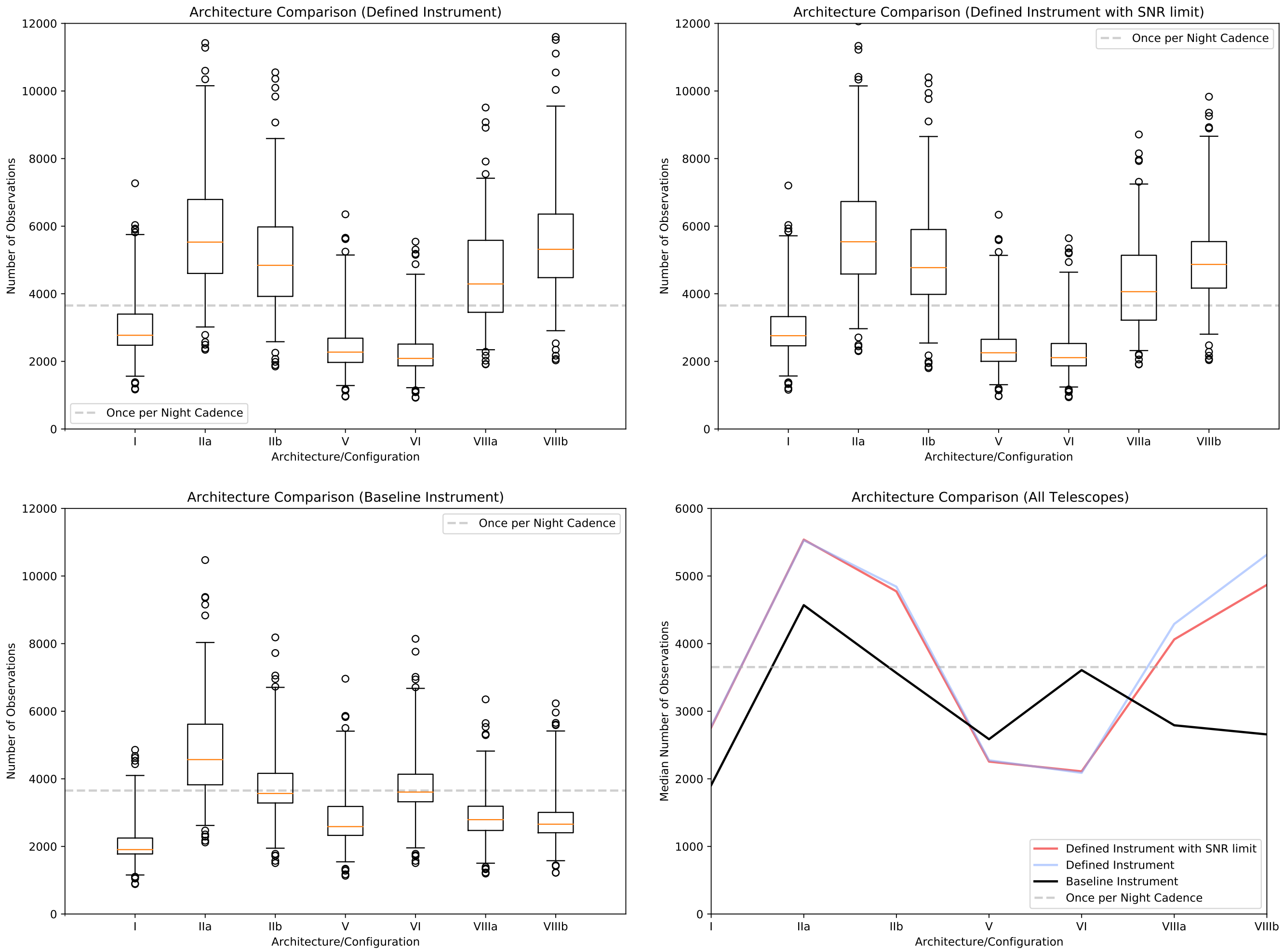

Figure 9. Top Left, Top Right, Bottom left: Comparison of the distribution of the number of observations between each architecture presented in §2.4 for the three spectrograph assumptions respectively: the champion-defined spectrograph with a RV precision photon noise requirement and no minimum SNR per spectral resolution element requirement, the champion-defined spectrograph with both a RV precision photon noise requirement and a minimum SNR per spectral resolution element requirement, and the baseline instrument spectrograph with only a RV precision photon noise requirement and no minimum SNR per spectral resolution element requirement. The boxes show the 25th/75th percentile, with the median marked in orange. The whiskers extend from the 5th to the 95th percentile. For all architectures, the number of observations is summed across all telescopes for the specified architecture. **Bottom Right:** Comparison of the median number of observations between each architecture presented in §2.4 for the three spectrograph and survey requirements combination assumptions considered: the champion-defined spectrograph with both a RV precision photon noise requirement and a minimum SNR per spectral resolution element requirement (red line), the champion-defined spectrograph with only a RV precision photon noise requirement and no minimum SNR per spectral resolution element requirement (blue line), and a baseline instrument spectrograph with only a RV precision photon noise requirement and no minimum SNR per spectral resolution element requirement (black line). The number of observations from an effective cadence of once per night per architecture (3653 epochs) is shown as a dashed horizontal line.

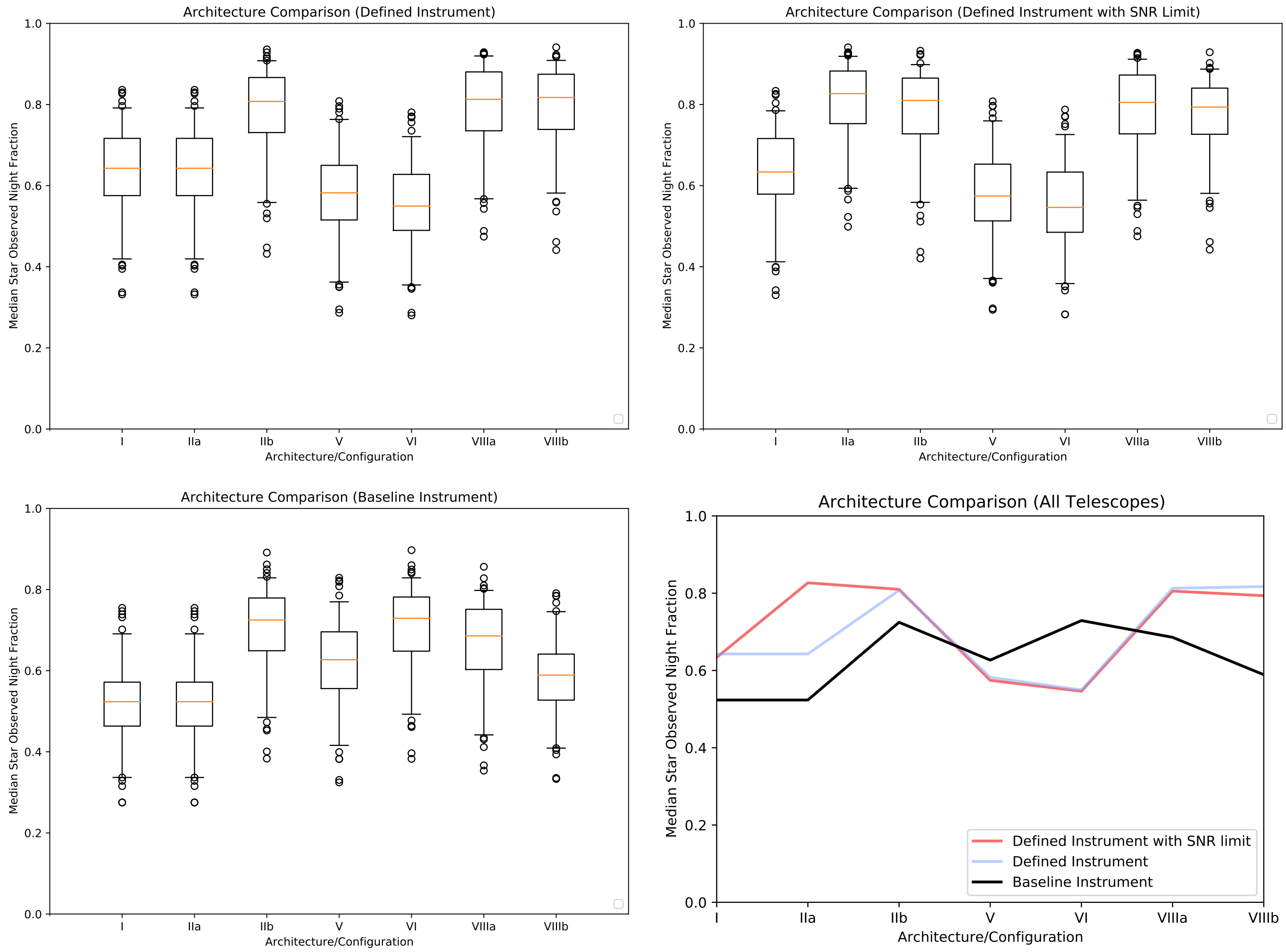

Figure 10. Comparison across architecture simulations for the observable nights fraction: the number of nights in which a star is observed divided by the number of nights that star could be observed. A value of 1 means that every night a star is observable by at least 1 telescope (e.g. not weathered out and above the pointing limits), at least 1 or more of the telescopes in the architecture does observe it in our simulations. If more than 1 telescope observes the same star on the same night, that star does not get double-counted, so the maximum possible fraction is 1.0. Given that each telescope site is modeled independently, we do not optimize this quantity (e.g., we do not prioritize a particular star at a given telescope higher if the other 2–5 telescopes are weathered out). The three box plots are for the distribution of observation fractions under different spectrograph instrument configurations as in Figure 9, while the line graph shows the medians for all. The color scheme is the same as Figure 9 as well. The observable nights fraction is effectively an approximate comparison of the survey efficiency for the given target list; not a single star in any architecture is observed every night it can be. For architectures VIIIa and b, nights where the telescopes with $<$100% time allocation were not used for the RV survey were not counted to penalize the architectures.

Finally, an efficient RV survey will need to minimize target slew and acquisition time, particularly for larger aperture telescopes. We consider the following limiting survey case: if all of the exposure times are limited by p-mode oscillation time-scales and not photon noise or SNR exposure time requirements, then each star would have a five minute target dwell time (see §2.3). Taking into consideration weather losses, slew and acquisition overhead, this limiting scenario would result in a survey with approximately ∼2500 observations on average per star per telescope. Thus, for a typical architecture with three telescopes per hemisphere, a p-mode oscillation time-scale limited exposure time survey would achieve ∼7500 observations per star. This number of observations is achieved for some of the most frequently observed targets in the architectures with >4-m apertures (IIa, IIb and VIIIa, VIIIb); for these telescopes and targets, the RV survey performance is limited by their minimum dwell times. However, we see that for the majority of the survey targets and architectures, even for the larger apertures, we are not limited by target dwell time, but rather the photon noise precision and SNR per resolution element exposure time requirements at this level of RV precision. This is distinctly different than the era of 1–3 m/s RV surveys, where the desired photon noise precision on large-aperture telescopes can be achieved within five minutes for most nearby, bright stars.

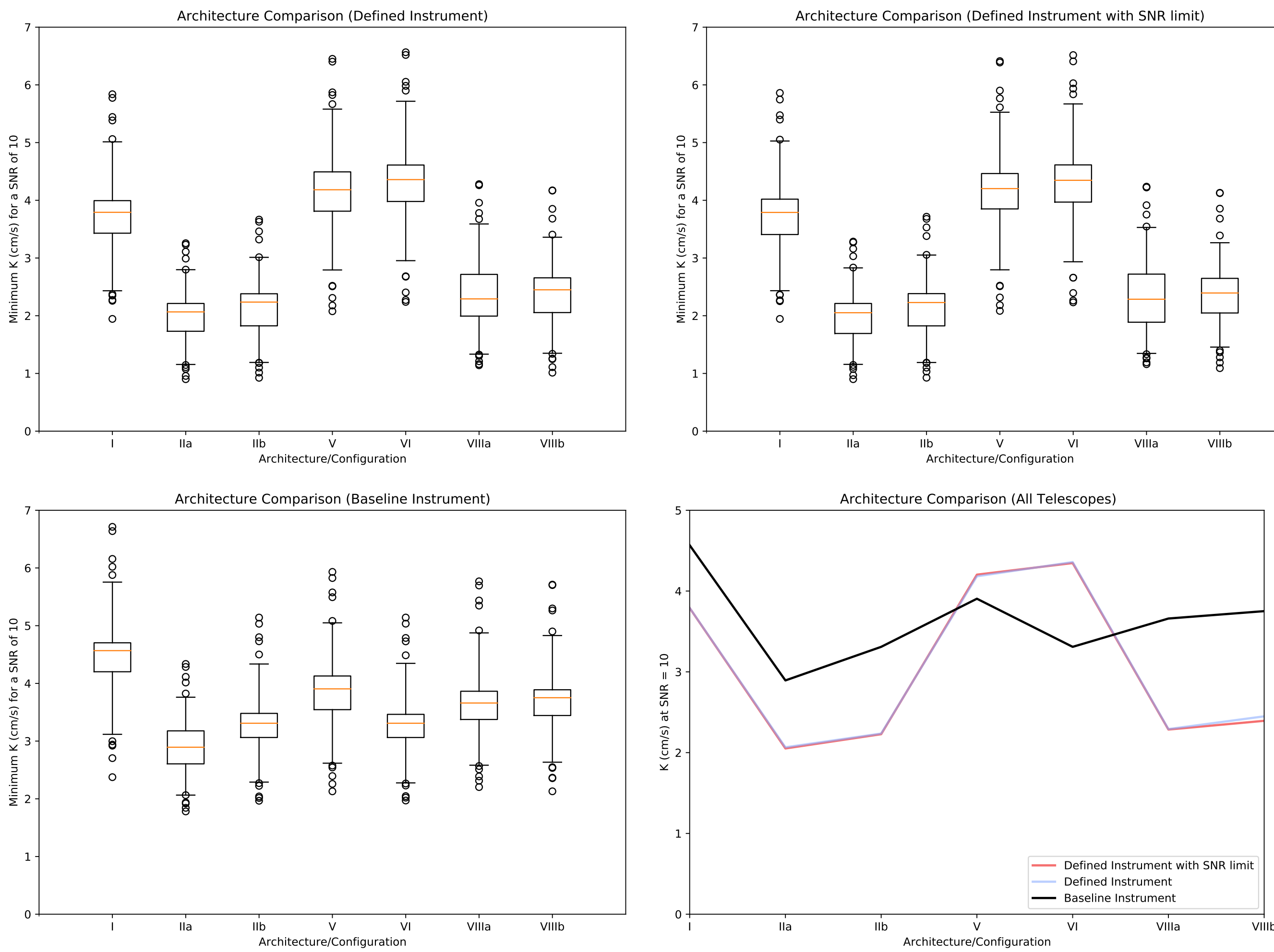

Figure 11. Comparison across architecture simulations for minimum reflex velocity semi-amplitude sensitivity at a nominal SNR of 10, as inferred from equations 1 and 2 for the number of observations per star and architecture single measurement precision. The box plots show the distribution of target stars under the different instrument configurations, while the line graph shows just the medians for all configurations, as in Figure 9.

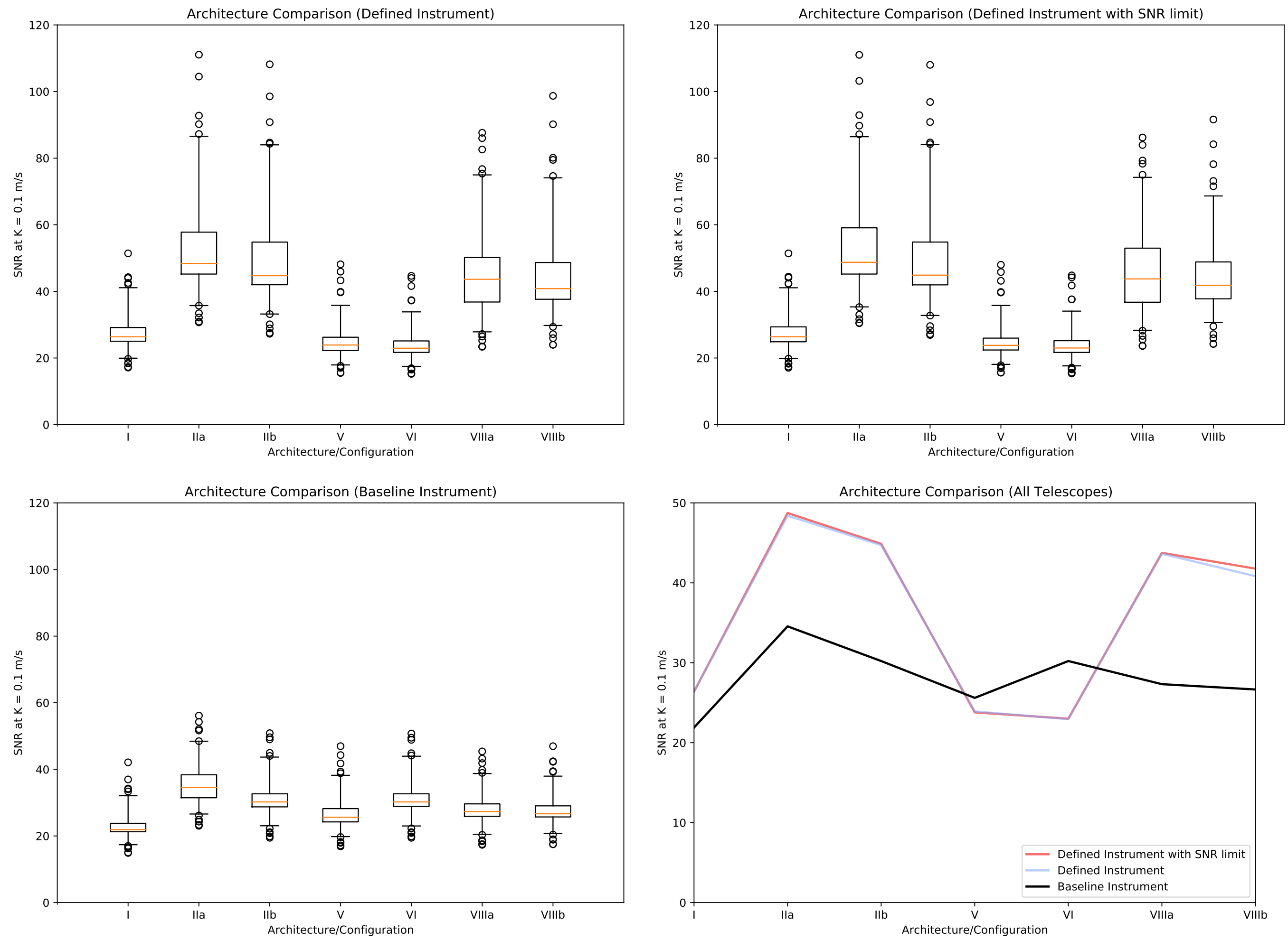

Figure 12. Comparison across architecture simulations for the maximum signal to noise ratio (SNR) for a planet detection at a nominal reflex velocity semi-amplitude of 0.1 m/s. The box plots show the distribution of target stars under the different instrument configurations, while the line graph shows just the medians for all configurations, as in Figure 9.

5. DISCUSSION

In this section, we discuss the relative performance of the architectures simulated herein, and we present an assessment in §5.1 of the impact of our survey simulation assumption on our results. First, using the baseline instrument spectrograph for all architectures, architecture IIa has the largest median number of observations per star due to having the most glass (on average). Architectures IIb and VI are close behind, with I, V, and VIII resulting in the fewest median number of observations per star. The sensitivity and SNR estimates follow from the number of observations per star; however the differences are more muted from these on account of the scaling with the square root of the number of observations. For the champion defined instruments, precision and wavelength coverage choices can have a large (about factor of 2) effect on number of observations per star. Including the instrument variations increase the spread in the number of observations per star and sensitivity estimates, with the architectures forming two distinct groups. Architectures IIa, IIb, VIIIa, and VIIIb are all in the high cadence/efficient/high sensitivity group, while architectures I, V, and VI are in the low sensitivity group for the reasons that vary between them – telescope aperture, spectrograph efficiency, spectral grasp, etc. As might be expected, larger apertures can compensate for lower throughput / spectral grasp, and vice-versa.

Second, efficient (close to nightly cadence) observations are improved with additional telescopes at additional sites, up to a point. The peak achieved median survey cadence appears to be a bit above 80% across the architectures considered, with all architecture achieving much lower cadences for some outlier stars. Presumably, a more sophisticated dispatch scheduler that coordinates the observing sequences across telescopes within an architecture could achieve a higher and more uniform cadence. However, we do not investigate that possibility herein.

Third, all architectures considered were able to achieve the SNR and semi-amplitude sensitivities sufficient to find "earth-like planets around sun-like stars" for most of the targets in the survey in the optimistic photon noise limiting scenario. This is due to a combination of: some of the assumptions being optimistic (see section 5.1), the relatively large number of telescopes compared to prior single-telescope RV surveys, most (and aside from architecture VIII, all) telescopes are assumed to be fully dedicated facilities, and the long survey duration of ten years. While several architectures failed to reach the equivalent of nightly cadence for most stars, even the down-scoped cases (less than 6 telescopes) had several hundred observations. Even though we did not consider the limiting impacts of stellar activity and correlated noise herein on the ability of these surveys to recovery Earth-mass analogs, with all variants of all architectures achieving several thousand observations per star, these architectures would gather sufficient data to enable the application of sophisticated stellar activity modeling.

5.1. *Survey simulation assumptions and their effects*

A number of simplifying assumptions were made for the survey simulations. In this sub-section, we categorize their effects as rendering these simulations optimistic, pessimistic, or neutral/ambiguous. We defer to a future work quantifying the impact of these assumptions.

Optimistic assumptions:

- Instrument design requirements can be achieved, including efficiency and instrumental noise as specified
- There is no degradation in throughput over the decade-long survey due to dust accumulation on the optics.
- Stellar activity can be mitigated completely, as no correlated noise models are included herein. This is investigated in Luhn et al. (in prep).
- Tellurics can be perfectly corrected.
- The exposure time calculator atmospheric model is possibly assumed to be more transparent than in practice, and no telluric absorption lines are included.
- Telescopes do not have significant downtime besides weather losses.
- Weather losses continue at historical rates; climate change effects may be increasing clouds/haze at most sites.

- Weather conditions night-to-night are uncorrelated, which will significantly impact any injection and recovery tests which are not explored herein.
- Time allocation is uniform; bright time gives additional limitations on when stars can be observed and introduce additional correlated sampling.

Pessimistic assumptions:

- Observatories at different sites do not coordinate and optimize target lists and prioritization.
- Telescope sizes, particularly for the architectures with the 4, 6, and 8 meter class observatories, are at the smaller end of each size class specified. For example, 3.5-m apertures are simulated for the architectures with 4-m class telescopes.
- Pointing limits; many telescopes can go below the 2 airmass/30 degree above the horizon limit that we assumed, which can extend the observing season duration of targets and minimize annual gaps.
- Site selection does not include any options in eastern Europe or Asia, and only existing sites were simulated.
- Target Selection: While the target list is consistent between architectures and all stars on it are "good", no attempt to further optimize the list to increase cadence/sensitivity or number of stars at a fixed cadence/sensitivity was done.

Ambiguous Assumptions:

- Throughput in existing instruments is assumed to be constant as a function of wavelength. We assume a median throughput instead of peak throughput to account for this effect.
- Constant spectrograph resolution. As with throughputs, we assume an intermediate value to reflect the overall system spectral resolution to account for this effect.
- NEID is the assumed baseline specifications for future instruments, particular for the detectors and spectral grasp.
- Site selection: a number of the chosen sites have alternatives far enough away to impact weather and declination effects, which were not optimized. Additionally, the large number and spread of sites mitigates the effects of any one site being good/bad.
- Survey timing: A ten year survey with all dedicated instruments mitigates any effects from a specific site having an unusually good/bad year in terms of open-dome time.

6. CONCLUSIONS

We developed simulations of a set possible next-generation global-network RV surveys with realistic site parameters. We generate exposure times for a given star, from its temperature, radius, distance, metallicity, surface gravity, and rotational velocity, as well as the properties of the telescope and instrument measuring it. We gathered the parameters for a nominal target list of nearby, bright stars common to future direct imaging mission concepts, several existing and potential observatory sites, and a set of telescope/instrument combinations. Through the results of these simulations, we estimated the distributions of observations per star, target observation frequency as a function of available nights, and approximate estimates of planet detection sensitivity. As expected, we find that the achieved cadences generally scaled with the collective telescope aperture. We find that most architectures considered herein can achieve the theoretical minimum (optimistic bound) number of observations required to detect at SNR=10 an Earth-mass analog producing a 9 cm/s stellar reflex velocity for all targets, with some margin to spare particularly for architectures II and VIII. Finally, we considered the major assumptions of the survey and how they could affect our results, which along with cost considerations can be explored in future work.

ACKNOWLEDGMENTS

Part of this research was carried out at the Jet Propulsion Laboratory, California Institute of Technology, under a contract with the National Aeronautics and Space Administration (80NM0018D0004).

PN and PP would like to acknowledge support from the JPL Exoplanet Exploration Program and NSF AAG 1716202 for this work.

URS300287 approved for unlimited release by NASA JPL with clearance number CL#21-2386

REFERENCES

Beatty, T. G., & Gaudi, B. S. 2015, PASP, 127, 1240

Chaplin, W. J., Cegla, H. M., Watson, C. A., Davies, G. R., & Ball, W. H. 2019, AJ, 157, 163

Gaudi, B. S., & Winn, J. N. 2007, ApJ, 655, 550

Gaudi, B. S., Seager, S., Mennesson, B., et al. 2020, arXiv e-prints, arXiv:2001.06683

Nava, C., Johnson, S., McCrady, N., & Minerva. 2015, in American Astronomical Society Meeting Abstracts, Vol. 225, American Astronomical Society Meeting Abstracts #225, 258.26

Newman, P. D. in prep

Robertson, P. M., Hearty, F. R., Anderson, T. B., et al. 2016, in Society of Photo-Optical Instrumentation Engineers (SPIE) Conference Series, Vol. 9908, Proc. SPIE, 990862

Schwab, C., Rakich, A., Gong, Q., et al. 2016, in Society of Photo-Optical Instrumentation Engineers (SPIE) Conference Series, Vol. 9908, Proc. SPIE, 99087H

Swift, J. J., Bottom, M., Johnson, J. A., et al. 2015, Journal of Astronomical Telescopes, Instruments, and Systems, 1, 027002

The LUVOIR Team. 2019, arXiv e-prints, arXiv:1912.06219

Vogt, S. S., Radovan, M., Kibrick, R., et al. 2014, PASP, 126, 359